공학석사학위논문

$La_2NiO_{4+\delta}$ 물질계의 이온/전자 열기전력과 산소의 열 이동특성

Ionic/Electronic Thermopower and Oxygen Thermotransport of Undoped $La_2NiO_{4+\delta}$

2014년 2월

서울대학교 대학원

재료공학부

이인범

Abstract

Ihnbeom Lee

Department of Material Science and Engineering

The Graduate School

Seoul National University

As technology develops to its cutting edge, environmental issue has emerged due to massive use of fossil fuel. To successfully cope with the global environmental problems, generating renewable green energy using Solid Oxide Fuel Cell is suggested as a pertinent alternative. Mixed Ionic Electronic Conductors (MIECs) are promising materials used in Solid Oxide Fuel Cell. In this context, mass/charge transport properties of MIECs are studied in order to understand their properties thoroughly.

As materials that are used in forming solid-state device and is utilized in pumping/separation application, MIEC has recognized its importance. In this study, $La_2NiO_{4+\delta}$ is used as a targeted MIEC because it has high ionic and electronic transport properties. Along with these properties, mass/charge transport properties under isothermal condition have been explored. Despite these efforts, mass/charge transport properties under non-isothermal condition have not been navigated thoroughly.

Throughout this work, mass/charge transport properties of this system under non-isothermal condition have measured by using two-probe ion blocking technique. By using this technique, ionic/electronic thermopowers are obtained and oxygen thermotransport of undoped $La_2NiO_{4+\delta}$ has been studied. For this oxide system, ionic thermopowers are measured. With

previously studied isothermal transport properties, 2x3 Onsager matrix is completed. Experiment of undoped $La_2NiO_{4+\delta}$ is performed in temperature range of 800 ~ 1000ºC as a function of □6<loga_{O_2}<0. Under these thermodynamic conditions, transient ionic thermopower and ionic/electronic thermopowers under Soret condition are measured. By using ionic/electronic thermopowers under Soret condition, non-isothermal transport coefficients are calculated. According to the nonisothermal transport coefficients, oxygen ion and hole appeared to be moving from relatively hotter side to colder side. Also, the effect of temperature difference to oxygen activity difference is calculated. When the temperature difference is about 100K, the effect to oxygen activity is approximately $\Delta\log a_{O_2}$ ~ 1.5. Also, term reduced heat of transport of oxygen, which gives insight to oxygen ion movement based on heat, is evaluated. Values of reduced heat of transport vary from -200 to 100 kJ/mole. At last, chemical potential variation from upper and bottom of specimen is studied in order to obtain deeper understanding of oxygen thermotransport.

Keywords: Mixed Ionic Electronic Conductor, Onsager transport coefficients, non-isothermal mass/charge transport properties, partial ionic/electronic thermopower, reduced heat of transport, oxygen thermotransport

Student Number: 2012-22543

Contents

List of Figures

(heater-on) and subsequent cooling (heater-off) at 1000ºC in $\log a_{O_2} = \log a_{O_2}^{ref}$ = -1.985±0.001. Here $\Delta T' = T_1 - T_4$; $\Delta T = T_2 - T_3$

Fig.IV.3. Typical temporal variation of (a) $\Delta\eta_e/F$, (b) $-\Delta(\eta_i - \mu_o^{ref})/F$, and (c) ΔT during heating (heater-on) and subsequent cooling (heater-off) at1000ºC in $\log a_{O_2} = \log a_{O_2}^{ref}$ = -1.985±0.001. Where $\Delta T = T_2 - T_3$.

Fig.IV.4. Behavior of (a) $\Delta\eta_e/F$, (b) $-\Delta(\eta_i - \mu_o^{ref})/F$ with respect to ΔT during heating (heater-on) and subsequent cooling (heater-off) at1000ºC in $\log a_{O_2} = \log a_{O_2}^{ref}$ = -1.985±0.001. Where $\Delta T = T_2 - T_3$.

Fig.IV.5. (a) $\Delta\eta_e/F$ and (b) $-\Delta(\eta_i - \mu_o^{ref})/F$ under Soret equilibrium with respect to at1000ºC in $\log a_{O_2} = \log a_{O_2}^{ref}$ = -1.985±0.001. Slope obtained from here indicates θ_e^{st} for (a) and $\theta_i^{st} - S_o^{ref}/2F$ for (b) where $\Delta T = T_2 - T_3$.

Fig.IV.6. (a) partial electronic thermopower under Soret condition, θ_i^{st}, and (b) partial electronic thermopower, θ_e^{st}, vs. $\log a_{O_2}$ at 1000ºC, 900ºC, and 800ºC.

Fig.IV.7. Isothermal Onsager transport coefficients vs. oxygen activity of $La_2NiO_{4+\delta}$ [21].

Fig.IV.8. Non-isothermal Onsager transport coefficients vs. oxygen activity of $La_2NiO_{4+\delta}$

Fig.IV.9. $\Delta \log a_{O_2}/\Delta T$ vs. $\log a_{O_2}$ for temperature 800ºC, 900ºC, and 1000ºC

Fig.IV.10. $-\Delta(\eta_i - \mu_o^{ref})/F$ behavior with respect to ΔT along with calculation of initial, θ^o, and steady state, θ^{st}, ionic thermopower. Cell condition was at1000ºC in $\log a_{O_2} = \log a_{O_2}^{ref}$ = -1.985±0.001 where $\Delta T = T_2 - T_3$.

Fig.IV.11. Initial and steady state ionic thermopower vs. $\log a_{O_2}$ at 1000ºC,

Fig.IV.20. $\Delta\mu_o$ calculated via Eq. (IV.15) from signals obtained from Fig.IV.16 vs. ΔT for (a) $\log a_{O_2}$ = -1.104 ± 0.001 ($q_o^* > 0$) and $\log a_{O_2}$ = -3.031 ± 0.001 ($q_o^* < 0$). Information retrieved from red line (initial transient state) refers to $-\bar{S}_o - q_o^*/T$ and information from blue line (steady state) refers to $-\bar{S}_o$, respectively.

List of Tables

I. Introduction

Among lots of issues prevailing these days, environmental problem is considered to be one of the major issues that must be overcome by human race. Such issues majorly arose due to massive fossil fuel use followed by increase in human population. As environmental problems emerged, fuel cell technology has been studied by researchers to solve rising issues. So, in order to efficiently use this technology, exploring a method to improve and develop properties of materials used has become an important issue. In fuel cell technology, hydrogen fuel is required. Hydrogen fuel can be generated via process of partial oxidation of methane. For partial oxidation of methane, supply of oxygen is crucial. To supply oxygen properly, feasible oxygen permeation membrane is required. Materials that are used in permeation membrane require high ionic and electronic conductivities because oxygen permeation efficiency is decided based on those properties. With these characteristics, materials used in permeation membrane are also spotlighted as cathode materials of intermediate-temperature solid oxide fuel cells (IT-SOFCs). In this manner, mixed ionic electronic conductor compounds attracted researchers due to their various usages in electrochemical applications: electrodes, electrolytes, gas separation membranes, sensors, atomic switches and memristors [1-4]. To get better insight to materials' fundamental characteristics, properties controlled by ionic and electronic species has been studied.

Comparative to generally known perovskite materials, $La_2NiO_{4+\delta}$ system (based on K_2NiF_4 crystal structure [5]) shows hyperstoichiometric property with oxygen interstitial (O_i'') and holes ($h^\bullet$). Also, oxygen ion move via oxygen interstitial sites [5-7]. Due to its applicability as oxygen permeation

membrane, it is important to understand its stability and oxygen permeation efficiency. For gas permeation membrane, equilibrium oxygen activities is decided based on air on one side and oxy-reforming/oxy-fuel combustion reaction on the other side. As a result of these exothermic reactions, temperature gradient is applied to the system. So, effect of temperature gradient upon the material must be studied to understand material's properties thoroughly.

It is well known that when the temperature gradient is applied to a uniform composition material, heat flux is generated from higher temperature side to relatively colder side. Induced heat flux generates mass flux indirectly as well as mass flux generated by the concentration gradient imposed directly [8]. Fick's law states that under isothermal condition, matter diffusion generally generated directly by concentration differences. Not only direct effect influences the system, indirect effect (concentration gradient generated by temperature gradient) can also be brought about upon the system. According to irreversible thermodynamics, a mass transport property is decided by two individual driving forces: electrochemical potential gradient and temperature gradient. So far, numerous studies have been performed using electrochemical potential gradient or chemical potential gradient as thermodynamic driving force. Comparatively, effect of temperature gradient upon system has been neglected and not been studied thoroughly. So, purpose of this work is to evaluate mass and charge transport properties under non-isothermal condition. To meet this purpose, initial and steady state thermoelectric power were measured. This work is meaningful in that kinetic information, such as reduced heat of transport and chemical diffusivity, are obtained based on ionic probe signal.

In Chapter II, fundamental properties of $La_2NiO_{4+\delta}$ system and theoretical backgrounds are reviewed. Then in Chapter III, experimental behavior of $La_2NiO_{4+\delta}$ under temperature gradient is shown. Then in Chapter IV, results are stated. At last, Chapter V, conclusions of this experiment are listed.

II. Literature Review

II.1. Crystal Structure of the Undoped $La_2N iO_{4+\delta}$ System

Structure of $La_2NiO_{4+\delta}$ system (K_2NiO_4 structure) is Ruddlesden Popper structure, m(AO)-n(ABO_3), with m=n=1. $La_2NiO_{4+\delta}$ system is consists of perovskite and rock salt layer which are stacked in sequence. Basic figure of $La_2NiO_{4+\delta}$ is shown in Fig.II.1 [5]. Within this structure, it is reported that rock salt layer, LaO^+, shows positive charge and perovskite layer, $La_2O_2^-$, has negative charge [9]. Ionic radii of $La_2NiO_{4+\delta}$ are listed in Table.II.1 [10].

Table.II.1. Lattice parameter and ionic radius of $La_2NiO_{4+\delta}$ [10]

Element	Ionic Radius (Å)
O	1.220
La	1.356
Ni	0.830

It is known that $La_2NiO_{4+\delta}$ structure contains oxygen interstitial defect [5, 11]. These systems have a polymorphism as a function of the temperature and oxygen nonstoichiometry [12]. For low temperature range of 0 to 500K, possibility of space groups such as Bmap, Pccn, Fmmm, and I4/mmm exist for this structure. Yet, for temperature at above 500K, the equilibrium crystal phase in this system is a tetragonal structure, which belongs to the I4/mmm space group. Phase diagram of this material is shown in Fig.II.2.

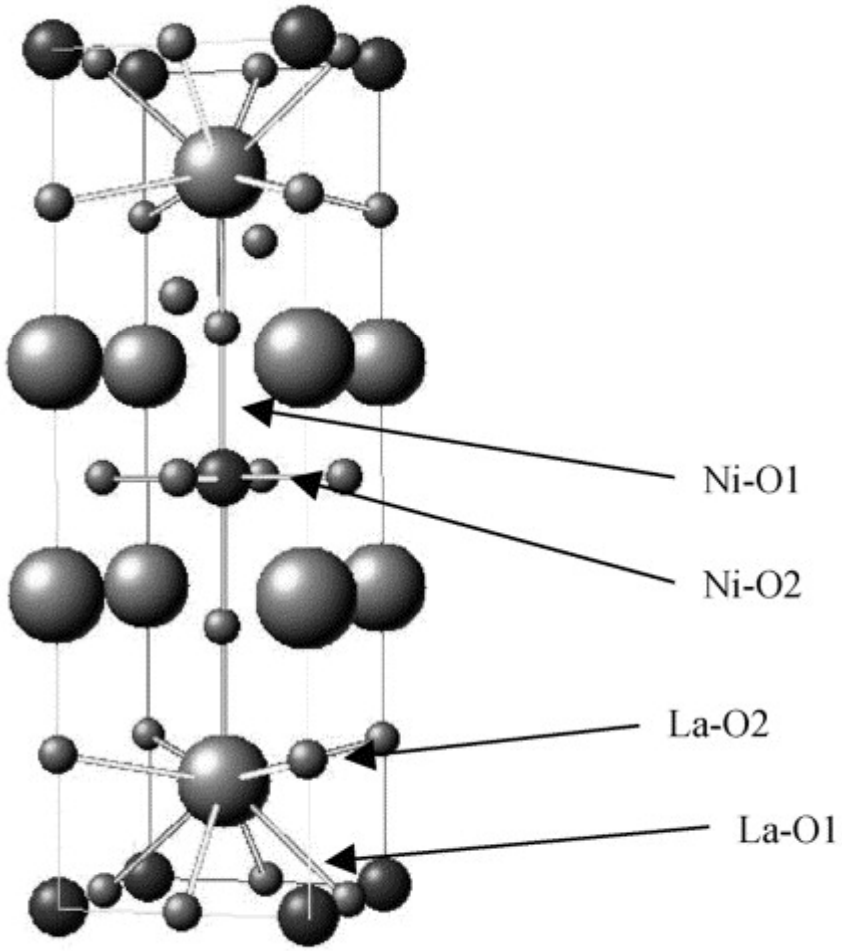

Fig.II.1.Crystal structure of $La_2NiO_{4+\delta}$ [5]

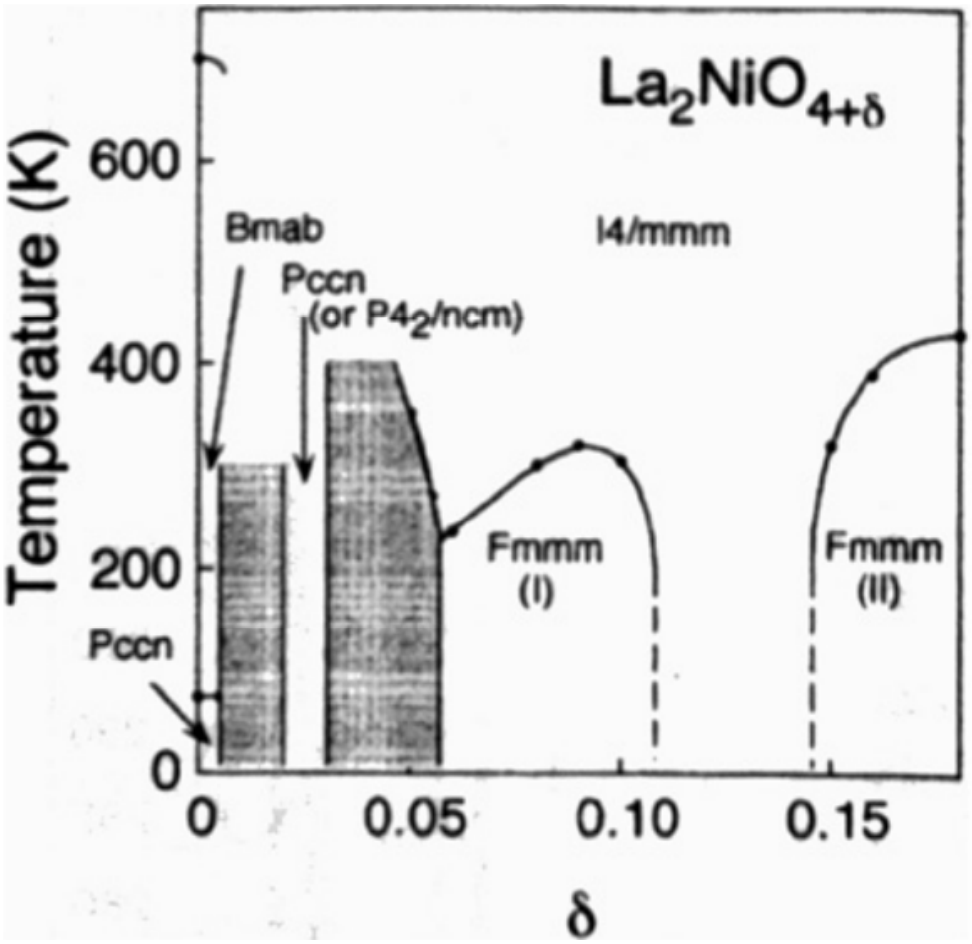

Fig.II.2. Phase diagram of $La_2NiO_{4+\delta}$ as a function of the temperature and oxygen nonstoichiometry [12]

II.2. Defect Structure of the Undoped $La_2NiO_{4+\delta}$ System

$La_2NiO_{4+\delta}$ system is well known to have intrinsic anti-Frenkel defect structure [6]. Compared to typical MIECs, $La_2NiO_{4+\delta}$ system is unusual in that under hyperstoichiometric area ($\delta > 0$). Under this condition, majority defects are oxygen interstitial, O_i'', and hole, $h^\bullet$ [5]. Also, oxygen vacancy concentration generated by anti-Frenkel defect within $La_2NiO_{4+\delta}$ is known to be negligibly small in amount [13]. Internal defect structure and external equilibrium reaction are written with mass action law as follows.

$$O_o + V_i = O_i'' + V_o'' \qquad ;K_F = [O_i''][V_o''] \tag{II.1}$$

$$0 = e' + h^\bullet \qquad ;K_i = np \tag{II.2}$$

$$\frac{1}{2}O_2 \leftrightarrow O_i'' + 2h^\bullet \qquad ;K_{ox} = [O_i''] + 2h^\bullet \tag{II.3}$$

Then Eqs. (II.1-3) are added with charge neutrality condition.

$$2[O_i''] + n = 2[V_o''] + p \tag{II.4}$$

With respect to oxygen activity, Brouwer diagram is shown in Fig.II.3 [14]. So far, major defect region of this system researched by researchers is $p = 2O_i''$ region of Fig.II.3. Under this region, La_2NiO_4 is showing p-type

semiconductor property. By assuming $La_2NiO_{4+\delta}$ is in p-type range, from Eqs. (II.1-3), following relation can be derived.

$$p = (K_{ox})^{1/3} P_{O_2}^{1/6} \tag{II.5}$$

$$\sigma \propto P_{o_2}^{1/6} \tag{II.6}$$

$\log\sigma$ increases in slope of 1/6 with respect to $\log Po_2$.

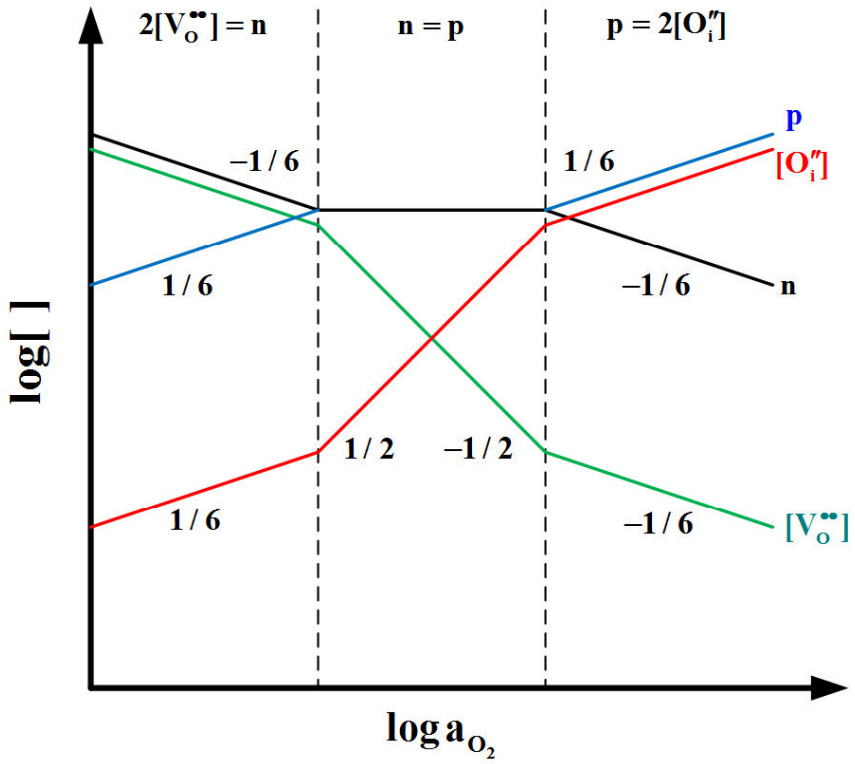

Fig.II.3. Brower diagram of La_2NiO_4 as a function of $loga_{O_2}$ [14]

II.3 Electrical and Ionic Conductivity and Oxygen Nonstoichiometry

Electrical and ionic conductivity of undoped $La_2NiO_{4+\delta}$ system are shown in Fig.II.4 [15] and Fig.II.5 [16]. As shown in Fig.II.4, electrical conductivity decreases as oxygen activity gets lower. This implies that main charge carrier of this system is a hole. As mentioned in Eq. (II.6), in most reducing atmospheres, the oxygen exponent "m" takes a value close to m=1/6 as evaluated from the ideal dilute solution model. But from previous study, $La_2NiO_{4+\delta}$ system is analyzed that it does not follow ideal dilute solution but shows positive deviation caused by the hole degeneracy [16]. From electrical conductivity results for undoped case, isothermal variation can be written as follows [16]:

$$\delta \propto a_{o_2}^{m} \tag{II.7}$$

Also by evaluating Onsager matrix in compounds, ionic conductivity is evaluated. In Fig.II.5 [16], partial ionic conductivity (σ_i) and conductivity with suppressed transfer of electrons (σ_i') are plotted with respect to oxygen activity. In this sense it is noted that $\sigma_i' > \sigma_i$ due to non-vanishing electron-ion cross effect.

By previous researchers, oxygen nonstoichiometry has been studied since it gives direct information of defect concentration. With oxygen nonstoichiometry, a positive deviation phenomenon is analyzed and its data is shown in Fig.II.6 [16].

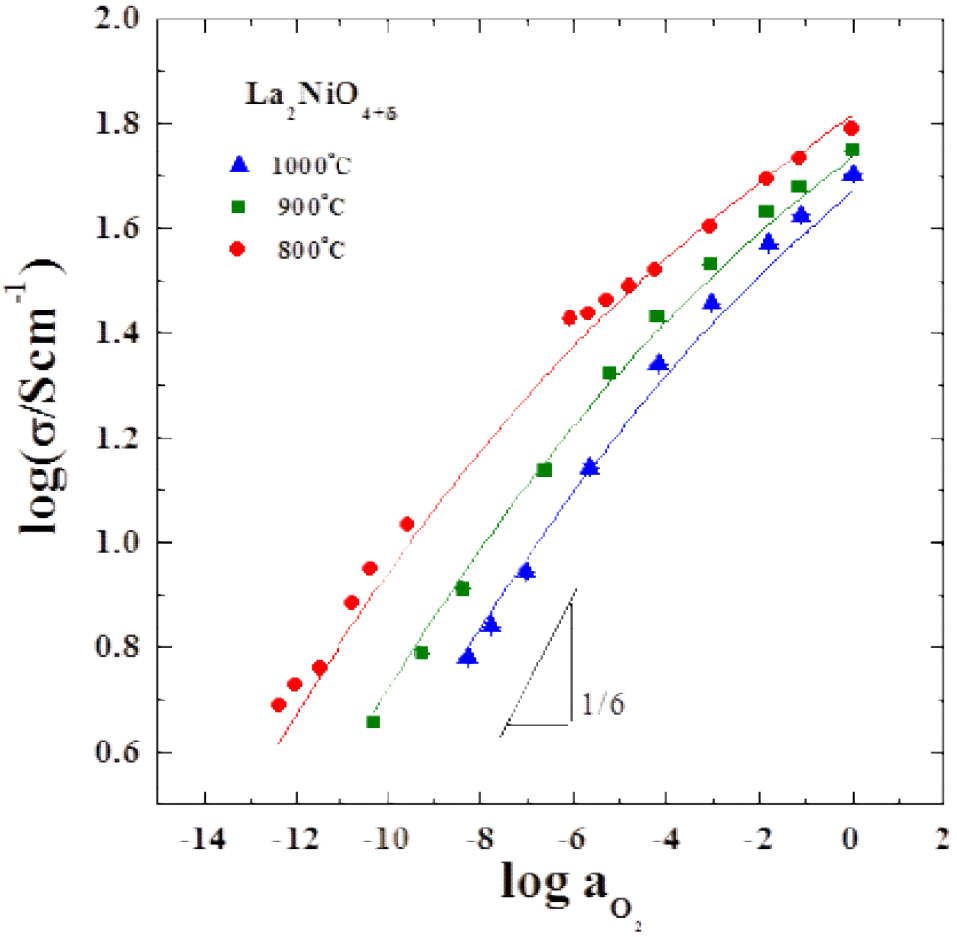

Fig.II.4. Electrical conductivity vs. oxygen activity of $La_2NiO_{4+\delta}$ at different temperatures. The triangle represents the ideal slope m=1/6. Solid lines are the best-fitted results [15]

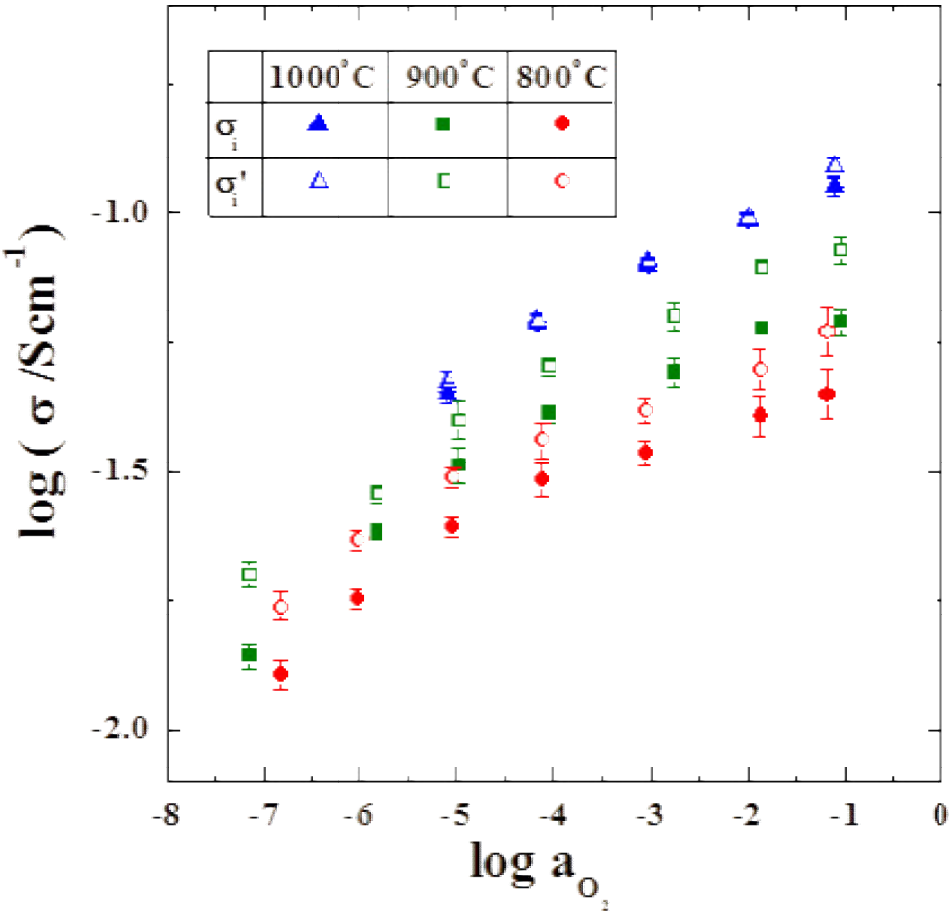

Fig.II.5. partial ionic conductivity (σ_i) and conductivity with suppressed transfer of electrons (σ_i') vs. oxygen activity of $La_2NiO_{4+\delta}$ at different temperatures [16]

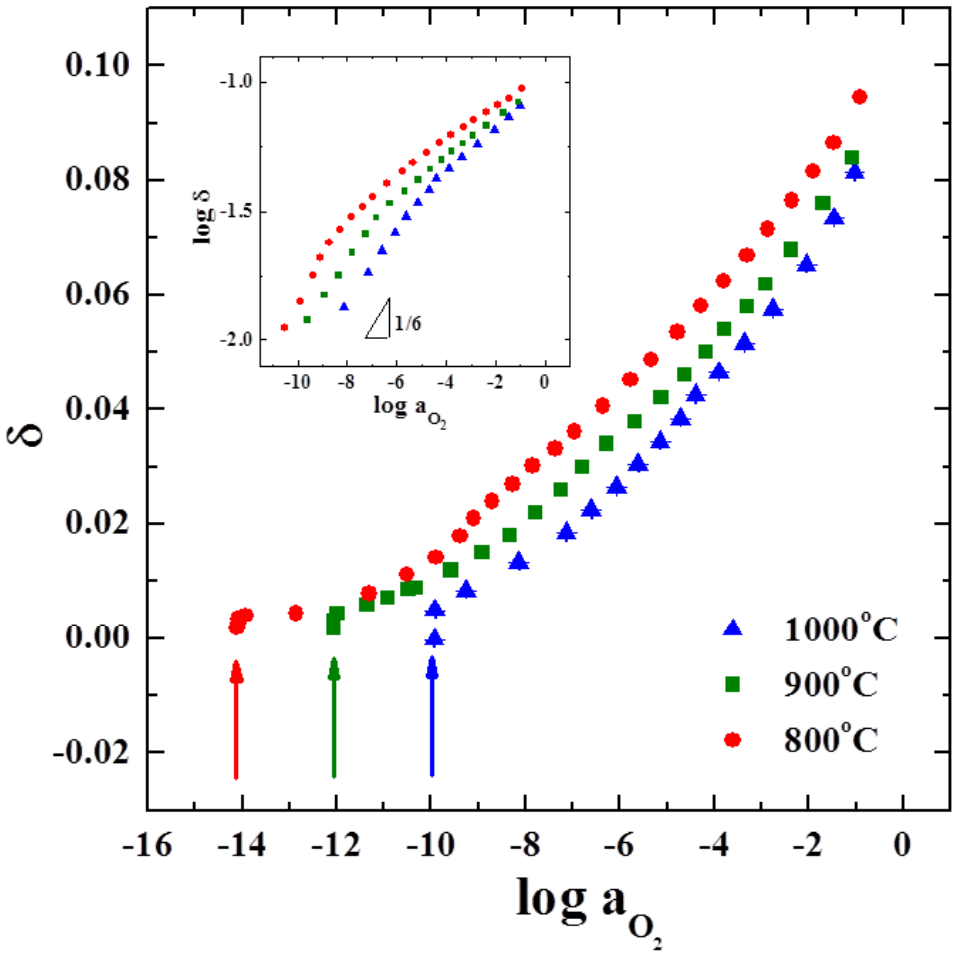

Fig.II.6. Oxygen nonstorichiometry δ vs. oxygen activity of undoped $La_2NiO_{4+\delta}$ in semi-logarithmic scale at 800ºC, 900ºC, and 1000ºC. Arrows indicate the stability limit of the undoped $La_2NiO_{4+\delta+}$[16]

II.4 Thermoelectric Voltage and Oxygen Thermotransport

Transport properties of mass and charge carrier under iso/non-isothermal conditions can be analyzed with irreversible thermodynamics. Mass and charge transport properties are studied started with de Groot's analysis [17].

Irreversible phenomena are induced by different kinds of driving forces, X_i (i=1,2,…,n). These irreversible phenomena appear in forms of flow density, J_i (i i=1,2,…,n), such as heat flow, diffusional flow, electrical flow, etc., which are known as flux, flow, current, etc. Relationship between these driving forces and flow density is shown as:

$$J_i = \sum_{k=1}^{n} L_{ik} X_k \qquad \text{(II.8)}$$

Eq. (II.8) represents that flux (J_i) of certain species not only depend on its own driving force (X_i) but also depend on other charge carriers' driving forces ($X_{k\neq i}$). Relationship between flux and carrier density can be explained by phenomenological transport coefficient, L_{ik}. Here, relation between carrier density and driving force of charge carrier itself can be explained by direct transport coefficient, L_{ii}. Also, flow generated by indirect driving force, such as temperature, can be explained by interference coefficient (cross coefficient, indirect coefficient), $L_{k\neq i}$. Onsager's fundamental theorem states that if proper choice is made for the fluxes and forces, the matrix of phenomenological coefficients L_{ik} is symmetrical.

$$L_{ik} = L_{ki} (i, k = 1, 2, ..., n) \qquad \text{(II.9)}$$

Energy (U) and matter (M) flow and their driving force (X) satisfying Eq. (II.9) is written as follows [17].

$$J_{\mathrm{U}} \equiv \Delta\dot{U}; X_{\mathrm{U}} \equiv \Delta\left(\frac{\partial S}{\partial U}\right)_{\mathrm{M}} \tag{II.10}$$

$$J_{\mathrm{M}} \equiv \Delta\dot{M}; X_{\mathrm{M}} \equiv \Delta\left(\frac{\partial S}{\partial M}\right)_{\mathrm{U}} \tag{II.11}$$

Here, U is energy, M is matter, and $\Delta\dot{U}$ is derivation of ΔU against time. When system possesses certain volume, following equation is valid:

$$\mathrm{T}\mathrm{d}S = \mathrm{d}U - \mu\mathrm{d}M \tag{II.12}$$

Here, μ refers to chemical potential. By using Eq. (II.10), (II.11), and (II.12), driving force can be obtained.

$$X_{\mathrm{U}} = \Delta\left(\frac{1}{T}\right) = -\frac{\Delta T}{T^2} \tag{II.13}$$

$$X_{\mathrm{U}} = -\Delta\left(\frac{\mu}{T}\right) \tag{II.14}$$

For two charge carrier system, relation between flux and driving force is explained with 3x3 Onsager matrix [15, 18, 19, 20].

$$\begin{pmatrix} J_i \\ J_e \\ J_Q \end{pmatrix} = \begin{pmatrix} L_{ii} & L_{ie} & L_{iQ} \\ L_{ei} & L_{ee} & L_{hQ} \\ L_{Qi} & L_{Qe} & L_{QQ} \end{pmatrix} \begin{pmatrix} X_i \\ X_e \\ X_Q \end{pmatrix} \quad \text{(II.15)}$$

Here, i, e, and Q each represent oxygen ion, hole, and heat. J_i, J_e, and J_Q each stands for ionic flux, hole flux, and heat flux, respectively. Driving force sufficing Eq.(II.9) can be expressed as follows [19]:

$$X_i = -T\nabla\left(\frac{\eta_i}{T}\right) = -\nabla\eta_i + \frac{\eta_i}{T}\nabla T \quad \text{(II.16)}$$

$$X_h = -T\nabla\left(\frac{\eta_e}{T}\right) = -\nabla\eta_e + \frac{\eta_e}{T}\nabla T \quad \text{(II.17)}$$

$$X_Q = -\frac{1}{T}\nabla T \quad \text{(II.18)}$$

Eqs. (II.16)-(II.18) are driving force when rate of entropy production is Tσ as Howard and Lidiard used.

Meanwhile, to understand the term heat of transport, following matrixes transformation is used [21]. First, matter flow matrix is defined.

$$J_M = \begin{pmatrix} J_i \\ J_e \end{pmatrix} \quad \text{(II.19)}$$

$$X_{\mathrm{M}} = \begin{pmatrix} X_{\mathrm{i}} \\ X_{\mathrm{e}} \end{pmatrix} \tag{II.20}$$

Then L-coefficients matrix is defined as follows:

$$L_{\mathrm{MM}} = \begin{pmatrix} \mathrm{L}_{\mathrm{ii}} & \mathrm{L}_{\mathrm{ie}} \\ \mathrm{L}_{\mathrm{ei}} & \mathrm{L}_{\mathrm{ee}} \end{pmatrix} \tag{II.21}$$

$$L_{\mathrm{MQ}} = \begin{pmatrix} \mathrm{L}_{\mathrm{iQ}} \\ \mathrm{L}_{\mathrm{hQ}} \end{pmatrix} \tag{II.22}$$

$$L_{\mathrm{MQ}} = \begin{pmatrix} \mathrm{L}_{\mathrm{Qi}} & \mathrm{L}_{\mathrm{Qh}} \end{pmatrix} \tag{II.23}$$

By Eqs. (II.21)-(II.23), Eq. (II.15) matrix can be transformed into as follows [21]:

$$\begin{pmatrix} J_{\mathrm{M}} \\ J_{\mathrm{Q}} \end{pmatrix} = \begin{pmatrix} \mathrm{L}_{\mathrm{MM}} & \mathrm{L}_{\mathrm{MQ}} \\ \mathrm{L}_{\mathrm{QM}} & \mathrm{L}_{\mathrm{QQ}} \end{pmatrix} \begin{pmatrix} X_{\mathrm{M}} \\ X_{\mathrm{Q}} \end{pmatrix} \tag{II.24}$$

To induce the term heat of transport, J_{M} and J_{Q} are written as follows by using Eq. (II.24) when $X_{\mathrm{Q}} = 0$.

$$J_{\mathrm{M}} = \mathrm{L}_{\mathrm{MM}} X_{\mathrm{M}} \tag{II.25}$$

$$J_{\mathrm{Q}} = \mathrm{L}_{\mathrm{QM}} X_{\mathrm{M}} \tag{II.26}$$

From Eq. (II.25), X_{M} can be written as,

$$X_{\mathrm{M}} = J_{\mathrm{M}} \mathrm{L}_{\mathrm{MM}}^{-1} \tag{II.27}$$

Then Eq. (II.27) is substituted into Eq. (II.26).

$$J_{\mathrm{Q}} = \left(\mathrm{L}_{\mathrm{MM}}^{-1} \mathrm{L}_{\mathrm{QM}}\right) J_{\mathrm{M}} = Q_{\mathrm{M}}^{*} J_{\mathrm{M}} \tag{II.28}$$

Finally, heat of transport ($\mathrm{Q}_{\mathrm{M}}^{*}$) can be written. By Eastman [22], heat of transport can be defined as the heat that material exchanges with surrounding when that matter moves within the system in order to maintain isothermal condition ($X_{\mathrm{Q}} = 0$) within the system. Using Eqs. (II.25), (II.26), and (II.28), following equation is induced [23]:

$$\mathrm{L}_{\mathrm{Q}} = Q_{\mathrm{M}}^{*} \mathrm{L}_{\mathrm{MM}} \tag{II.29}$$

Then by substituting Eq. (II.21) and (II.23) into Eq.(II.29), relation between

isothermal transport coefficient, L_{km} (k, m=i, e), non-isothermal transport coefficient L_{Qk} (k=i, h), and heat of transport of species k, Q_k^* (k=i, e) can be written as:

$$\begin{pmatrix} L_{Qi} & L_{Qh} \end{pmatrix} = \begin{pmatrix} Q_i^* & Q_h^* \end{pmatrix} \begin{pmatrix} L_{ii} & L_{ie} \\ L_{ei} & L_{ee} \end{pmatrix} \tag{II.30}$$

Eq. (II.30) shows that isothermal transport coefficients and non-isothermal transport coefficients is related to each other by term heat of transport. As previously mentioned, heat of transport is defined as heat transported by matter while moving within the system. In order for the matter to move within the system, enthalpy (energy required for matter to gain certain space) is required. So, heat of transport can be divided into two parts: enthalpy and reduced heat of transport, q_k^*, [17, 19, 24, 25].

$$Q_k^* = q_k^* + \overline{H}_k \tag{II.31}$$

Here, $\overline{H}_k$ is defined as partial molar enthalpy of species k.

Meanwhile, heat of transport measurement is experimentally difficult. Comparatively, reduced heat of transport can be achieved experimentally. So to transform Eq. (II.15) into experimentally feasible matrix, by substituting Eq. (II.30), following relation is derived [17, 19, 24, 25].

$$J_{\mathrm{k(k=i,e)}} = \sum_{\mathrm{m=i,e}} \mathrm{L_{km}} (X_{\mathrm{m}} + Q_{\mathrm{m}}^{*} X_{\mathrm{Q}}) \tag{II.32}$$

Then by substituting driving force from Eqs. (III.26-28), Eq. (II.33) is achieved.

$$J_{\mathrm{k(k=i,e)}} = \sum_{\mathrm{m=i,e}} \mathrm{L_{km}} \left[-\nabla \eta_{\mathrm{m}} + \left(\eta_{\mathrm{m}} - Q_{\mathrm{m}}^{*} \right) \frac{\nabla T}{T} \right] \tag{II.33}$$

Then with Eq. (II.30), Eq. (II.33) transforms into as follows.

$$J_{\mathrm{k(k=i,e)}} = \sum_{\mathrm{m=i,e}} \mathrm{L_{km}} \left[-\nabla \eta_{\mathrm{m}} + \left(\eta_{\mathrm{m}} - \overline{H}_{\mathrm{m}} - q_{\mathrm{m}}^{*} \right) \frac{\nabla T}{T} \right] \tag{II.34}$$

Since $\eta_{\mathrm{m}} - \overline{H}_{\mathrm{m}} = -T\overline{S}_{\mathrm{m}}$, Eq. (II.34) is separated into two parts as shown in Eq. (II.35). Here, constant used for ∇T is defined as non-isothermal transport coefficient, $\mathrm{L_{kT}}$. This is different from $\mathrm{L_{kQ}}$ of Eq. (II.15).

$$J_{\mathrm{k(k=i,e)}} = -\sum_{\mathrm{m=i,e}} \mathrm{L_{km}} \nabla \eta_{\mathrm{m}} - \mathrm{L_{kT}} \nabla T \tag{II.35}$$

$$\mathrm{L_{kT(k=i,e)}} = \sum_{\mathrm{m=i,e}} \mathrm{L_{km}} \left(\overline{S}_{\mathrm{m}} + \frac{q_{\mathrm{m}}^{*}}{T} \right) \tag{II.36}$$

Then 2x3 transport coefficient matrix is shown as follows.

$$\begin{pmatrix} J_{\mathrm{i}} \\ J_{\mathrm{h}} \end{pmatrix} = -\begin{pmatrix} \mathrm{L_{ii}} & \mathrm{L_{ie}} & \mathrm{L_{iT}} \\ \mathrm{L_{ei}} & \mathrm{L_{ee}} & \mathrm{L_{hT}} \end{pmatrix} \begin{pmatrix} \nabla\eta_{\mathrm{i}} \\ \nabla\eta_{\mathrm{e}} \\ \nabla T \end{pmatrix} \tag{II.37}$$

Here, under isothermal condition (∇T=0), fluxes (J_{I}, J_{e}) and their driving forces ($\nabla\eta_{\mathrm{i}}$, $\nabla\eta_{\mathrm{e}}$) are conjugated parameter that meets Onsager reciprocal relation where $\mathrm{L_{ie}} = \mathrm{L_{ei}}$.

Eq. (II.36) shows that non-isothermal transport coefficient can be expressed in terms of isothermal transport coefficients and transported entropy ($\overline{\overline{S}}_{\mathrm{k}}$) [27]. Transported entropy here is defined as follows [27].

$$\overline{\overline{S}}_{\mathrm{k}} \equiv \overline{S}_{\mathrm{k}} + \frac{q_{\mathrm{k}}^{*}}{T} \tag{II.38}$$

Transported entrop can be written in forms of thermopower of ion and hole under Soret condition [28-30]. Under Soret condition, there is no mass/charge transport in equilibrium state that J_{i}=J_{h}=0. So, by substituting this boundary condition into Eq. (II.37) with α_{i}^{*} and α_{e}^{*} [31, 32], relation is shown as follows.y

$$\nabla\eta_{\mathrm{i}} + \overline{\overline{S}}_{\mathrm{i}}\nabla T + \alpha_{\mathrm{i}}^{*}\left(\nabla\eta_{\mathrm{e}} + \overline{\overline{S}}_{\mathrm{e}}\nabla T\right) = 0 \tag{II.39}$$

$$\alpha_{\mathrm{e}}^{*}\left(\nabla\eta_{\mathrm{i}}+\overline{\overline{S}}_{\mathrm{i}}\nabla T\right)+\nabla\eta_{\mathrm{e}}+\overline{\overline{S}}_{\mathrm{e}}\nabla T=0 \tag{II.40}$$

Then by subtracting α_{i}^{*} times Eq. (II.40) from Eq. (II.39), following equation is acquired.

$$\left(1-\alpha_{\mathrm{i}}^{*}\alpha_{\mathrm{e}}^{*}\right)\times\left(\nabla\eta_{\mathrm{i}}+\overline{\overline{S}}_{\mathrm{i}}\nabla T\right)=0 \tag{II.41}$$

Similarly, by subtracting α_{h}^{*} times Eq. (II.39) from Eq. (II.40), result is shown as follows.

$$\left(1-\alpha_{\mathrm{i}}^{*}\alpha_{\mathrm{e}}^{*}\right)\times\left(\nabla\eta_{\mathrm{h}}+\overline{\overline{S}}_{\mathrm{i}}\nabla T\right)=0 \tag{II.42}$$

Then following relation can be induced.

$$\left(\frac{\nabla\eta_{\mathrm{k}}}{\nabla T}\right)_{\mathrm{J_o}=0}=-\overline{\overline{S}}_{\mathrm{k}} \tag{II.43}$$

Meanwhile, thermopower under Soret equilibrium can be expressed as Wagner [27] suggested.

$$\theta_k^{st} = \frac{1}{z_k F}\left(\frac{d\eta_k}{dT}\right) = -\frac{1}{z_k F}\bar{\bar{S}}_k \qquad \text{(II.44)}$$

Here, superscript 'st' stands for steady state. In closed system with temperature gradient, change in oxygen nonstoichiometry shows time dependency since nonstiochiometry depends on chemical diffusion. So, thermopower can be shown as function of time. Superscript is used to distinguish thermopower under Soret condition from other time dependent thermopower. By using Eq. (II.36), (II.39), and (II.44), non-isothermal transport coefficient can be expressed as follows.

$$L_{kq} = -\sum_{m=i,e} L_{km}\left(z_m F \theta_m^{st}\right) \qquad \text{(II.45)}$$

With Chipman's [28] definition, Soret effect is "When a solution is maintained for some time in a temperature gradient, the upper part being warmer than lower, a difference in concentration in the two part is set up." Here the term "some time" refers to the fact that concentration gradient is in function of time for Soret experiment. Time dependency of concentration gradient has been reported by Agar [33] by suggesting analytic solution. Agar witnessed electromotive force change with respect to time when reaching Soret equilibrium [34]. Recently, Janek and Korte performed experiment and briefly reported thermoelectric voltage and thermopower's time dependency [35-37]. From initial and steady state thermopower, they retrieved reduced heat of transport. Based on their analysis, reduced heat of

transport values are obtained in this work.

With local equilibrium reaction, Eq. (II.46), flux of oxygen ion (i) and hole (h) can be written as Eq. (II.47) and (II.48) from Eq. (II.37).

$$\frac{1}{2}\mathrm{O}_2 \leftrightarrow \mathrm{O}^{2-} + 2\mathrm{h}^{+}; \nabla\mu_{\mathrm{o}} = \nabla\eta_{\mathrm{i}} + 2\nabla\eta_{\mathrm{e}} \tag{II.46}$$

$$J_{\mathrm{i}} = -\mathrm{L}_{\mathrm{ii}}\nabla\mu_{\mathrm{o}} + \left(2\mathrm{L}_{\mathrm{ii}} - \mathrm{L}_{\mathrm{ih}}\right)\nabla\eta_{\mathrm{e}} - \mathrm{L}_{\mathrm{iT}}\nabla T \tag{II.47}$$

$$J_{\mathrm{e}} = -\mathrm{L}_{\mathrm{ie}}\nabla\mu_{\mathrm{o}} + \left(2\mathrm{L}_{\mathrm{ei}} - \mathrm{L}_{\mathrm{ee}}\right)\nabla\eta_{\mathrm{e}} - \mathrm{L}_{\mathrm{eT}}\nabla T \tag{II.48}$$

Then with open circuit condition Eq. (II.49) and Eq. (II.50) are acquired.

$$-2\mathrm{F}J_{\mathrm{i}} + \mathrm{F}J_{\mathrm{e}} = 0 \tag{II.49}$$

$$\nabla\eta_{\mathrm{e}} = \mathrm{f}\nabla T + \frac{\mathrm{t}_{\mathrm{i}}}{2}\nabla\mu_{\mathrm{o}} \tag{II.50}$$

Definition of t_i, transference number, is given in Eq. (II.51) [32] and f is defined as in Eq. (II.52).

$$t_i = \frac{z_i F J_i}{\sum_{k=i,e} z_k F J_k} = \frac{2(2L_{ii} - L_{ie})}{4L_{ii} + L_{ee} - 4L_{ie}} \tag{II.51}$$

$$f = \frac{2L_{iT} - L_{eT}}{4L_{ii} + L_{ee} - 4L_{iT}} = \frac{1}{2} t_i \bar{\bar{S}}_i - t_e \bar{\bar{S}}_e \tag{II.52}$$

Then chemical potential gradient $\nabla \mu_o$ can be expressed as follows.

$$\nabla \mu_o = \left(\frac{\partial \mu_o}{\partial \delta} \right)_T \nabla \delta + \left(\frac{\partial \mu_o}{\partial T} \right)_\delta \nabla T = \left(\frac{\partial \mu_o}{\partial \delta} \right)_T \nabla \delta - \bar{S}_o \nabla T \tag{II.53}$$

Where δ is oxygen nonstoichiometry. Also, partial molar entropy and reduced heat of transport has following relations [27].

$$\bar{S}_o = \bar{S}_i + 2\bar{S}_e \tag{II.54}$$

$$q_o^* = q_i^* + 2q_e^* \tag{II.55}$$

With Eq. (II.38) and Eqs. (II.50)-(II.55), Eqs. (II.56) and (II.57) are derived.

$$\nabla \eta_i = t_e \left(\frac{\partial \mu_o}{\partial \delta} \right)_T \nabla \delta - \left(\bar{\bar{S}}_i - t_e \frac{q_o^*}{T} \right) \nabla T \tag{II.56}$$

$$\nabla\eta_e = \frac{t_i}{2}\left(\frac{\partial\mu_o}{\partial\delta}\right)_T \nabla\delta - \left(\bar{\bar{S}}_e - \frac{t_i}{2}\frac{q_o^*}{T}\right)\nabla T \tag{II.57}$$

In initial state when (t → 0), concentration redistribution (result from chemical diffusion) is negligible that $\nabla\delta(t \to 0) = 0$. By using this condition with Eqs. (II.56) and (II.57), Eqs. (II.58) and (II.59) are obtained.

$$\nabla\eta_i(t \to 0) = -\left(\bar{\bar{S}}_i - t_e\frac{q_o^*}{T}\right)\nabla T \tag{II.58}$$

$$\nabla\eta_e(t \to 0) = -\left(\bar{\bar{S}}_e - \frac{t_i}{2}\frac{q_o^*}{T}\right)\nabla T \tag{II.59}$$

Thermopower is defined as Eq. (II.60) using Wagner's [27] definition. With Eq. (II.60), Eqs. (II.58) and (II.59) are transformed into Eqs. (II.61) and (II.62).

$$\theta_k \equiv \frac{1}{z_k F}\left(\frac{d\eta_k}{dT}\right) \tag{II.60}$$

$$\theta_i^o = \frac{1}{2F}\left(\bar{\bar{S}}_i - t_h\frac{q_o^*}{T}\right) \tag{II.61}$$

$$\theta_e^o = -\frac{1}{F}\left(\bar{\bar{S}}_e - \frac{t_i}{2}\frac{q_o^*}{T}\right) \tag{II.62}$$

Superscirpt ‘o’ here refers to initial state where (t→0). So with Eq. (II.44) which is thermopower under Soret condition, difference between initial and steady state thermopower can be written in terms of reduced heat of transport [23].

$$\theta_{\mathrm{i}}^{\mathrm{st}} - \theta_{\mathrm{i}}^{\mathrm{o}} = -\frac{1}{2\mathrm{F}}\mathrm{t_e}\frac{q_{\mathrm{o}}^{*}}{T} \tag{II.63}$$

$$\theta_{\mathrm{e}}^{\mathrm{st}} - \theta_{\mathrm{e}}^{\mathrm{o}} = \frac{1}{2\mathrm{F}}\mathrm{t_i}\frac{q_{\mathrm{o}}^{*}}{T} \tag{II.64}$$

So if t_h or t_i is given for the system ($t_h + t_i = 1$), from difference between initial thermopower and that of Soret condition, reduced heat of transport can be calculated. Also, from information contents retrieved from thermocell, kinetic behaviors within system are analyzed. To understand transport properties of the system, electronic and ionic thermoelectric voltages’ analytical solutions given by T. W. Lee are used [23].

$$\begin{aligned}\frac{\Delta\eta_{\mathrm{e}}(\mathrm{t})}{\mathrm{F}} = &-\frac{1}{\mathrm{F}}\bar{\bar{S}}_{\mathrm{e}}\Delta T(\mathrm{t}) + \frac{\mathrm{t_i}}{2\mathrm{F}}\frac{q_{\mathrm{o}}^{*}}{T}\frac{\mathrm{L}}{l}\left[\Delta T(\mathrm{t}) - \Delta\mathrm{T^o}\right] \\ &\times\left\langle\frac{8}{\pi^2}\sum_{\mathrm{n=1}}^{\infty}\sin\left[\frac{(2\mathrm{n}-1)}{2}\pi\right]\left[\frac{(2\mathrm{n}-1)}{2}\pi\frac{l}{\mathrm{L}}\right]\Theta(\mathrm{t})\right\rangle\end{aligned} \tag{II.65}$$

$$\begin{aligned}-\frac{\Delta\eta_{\mathrm{i}}(\mathrm{t})}{\mathrm{F}} = &-\frac{1}{2\mathrm{F}}\bar{\bar{S}}_{\mathrm{i}}\Delta\mathrm{T}(\mathrm{t}) + \frac{\mathrm{t_e}}{2\mathrm{F}}\frac{q_{\mathrm{o}}^{*}}{T}\frac{\mathrm{L}}{l}\left[\Delta T(\mathrm{t}) - \Delta\mathrm{T^o}\right] \\ &\times\left\langle\frac{8}{\pi^2}\sum_{\mathrm{n=1}}^{\infty}\sin\left[\frac{(2\mathrm{n}-1)}{2}\pi\right]\left[\frac{(2\mathrm{n}-1)}{2}\pi\frac{l}{\mathrm{L}}\right]\Theta(\mathrm{t})\right\rangle\end{aligned} \tag{II.66}$$

Here, $\Theta(t)$ corresponds to as follows.

$$\Theta(t)=\left[\frac{1}{(2n-1)^2}-\frac{1}{(2n-1)^2-\omega^{T}\omega^{-1}}\right]\left\{\frac{\exp\left[-(2n-1)\omega t\right]-\exp(-\omega^{T}t)}{1-\exp(-\omega^{T}t)}\right\} \quad \text{(II.67)}$$

ω is relaxation frequency which is $\omega=\pi^2\widetilde{D}_o/L^2$. Eqs. (II.65)-(II.67) are used to obtain kinetic information by best-fitted curve. To understand the meaning of Eq. (II.66) and (II.67), two limiting cases are set up; i) temperature redistribution is very fast compare to chemical diffusion ($\omega^{T}>>\omega$), ii) vice versa ($\omega^{T}<<\omega$) [38]. In case i), with Eqs. (II.60), (II.65), (II.66), and (II.67), thermopowers of initial and steady state are derived.

$$\theta_e^{o}=\frac{1}{F}\left[\frac{d\Delta\eta_e(t\to 0)}{d\Delta T(t\to 0)}\right]=-\frac{1}{F}\left(\overline{\overline{S}}_e-\frac{t_i}{2}\frac{q_o^{*}}{T}\right) \quad \text{(II.68)}$$

$$\theta_i^{o}=-\frac{1}{F}\left[\frac{d\Delta\eta_i(t\to 0)}{d\Delta T(t\to 0)}\right]=\frac{1}{2F}\left(\overline{\overline{S}}_i-t_e\frac{q_o^{*}}{T}\right) \quad \text{(II.69)}$$

$$\theta_e^{st}=\frac{1}{F}\left[\frac{d\Delta\eta_e(t\to \infty)}{d\Delta T(t\to \infty)}\right]=-\frac{1}{F}\overline{\overline{S}}_e \quad \text{(II.70)}$$

$$\theta_i^{st}=-\frac{1}{2F}\left[\frac{d\Delta\eta_i(t\to \infty)}{d\Delta T(t\to \infty)}\right]=\frac{1}{2F}\overline{\overline{S}}_i \quad \text{(II.71)}$$

Unlike case i), in case ii), chemical diffusion is so fast that only

thermopower under Soret equilibrium can be obtained [23].

Solid state transport as a mechanism of oxygen thermomigration has been studied only for few oxide systems. It has been studied that oxygen redistribution generated can be interpreted as an electrochemical mass transport phenomenon caused by thermoelectric power [38]. Oxygen thermomigration can be explained by thermopower and heat of transport. Despite the efforts, researches on thermal diffusion still have not shown satisfying results and data acquired from researchers are in discord with each other [39].

III. Experimental

III.1. Sample Preparation

Preparation of undoped $La_2NiO_{4+\delta}$ power is based on modified Pechini method. This method is atomic scale reaction that precise cationic ratio can be obtained. Starting powers are dissolved in deionized water which are as follows: $La(OH)_3$ (99.9%, Aldrich, USA), $NiCO_3 2Ni(OH)_2 \bullet 4H_2O$ (99.9% Junsei, Japan), and H_5DTPA (98%, Aldrich, USA). Here, H_5DTPA refers to diethylenetriaminepentaacitic acid where total cations' mole ratio to H_5DTPA's mole ratio was set to be 3.0:1.7. Temperature is set to be 90ºC with heater and stirring bar is used. After time, change in color appears from opaque greenish color in to clear blue color as shown in Fig.III.2.1. After drying process, solid complex is pulverized and calcined at 900ºC for 2 hours with temperature increase rate of 3ºC per minute. Then powder is grinded again using mortar then placed in round mold to manipulate its form followed by cold isostatic pressing (CIP) at 200MPa. Lastly specimen is sintered at 1350ºC for 4 hours where increasing and decreasing time are each 7.5hours. After sintering, relative density of 95±1% specimen is obtained. XRD (Bruker D5005, Germany) data is shown in Fig III.2.2. Then via diamond suspension with particle size of 1μm, surface of specimen is polished.

(a)

(b)

Fig. III.1. Change in color of liquid mixture: (a) initial mixture before heating, (b) mixture after 40minutes at 90ºC, (c) mixture after 70minutes at 90ºC, and (d) mixture after 130minutes at 90ºC (the final color)

(c)

(d)

Fig. III.1. (Continued)

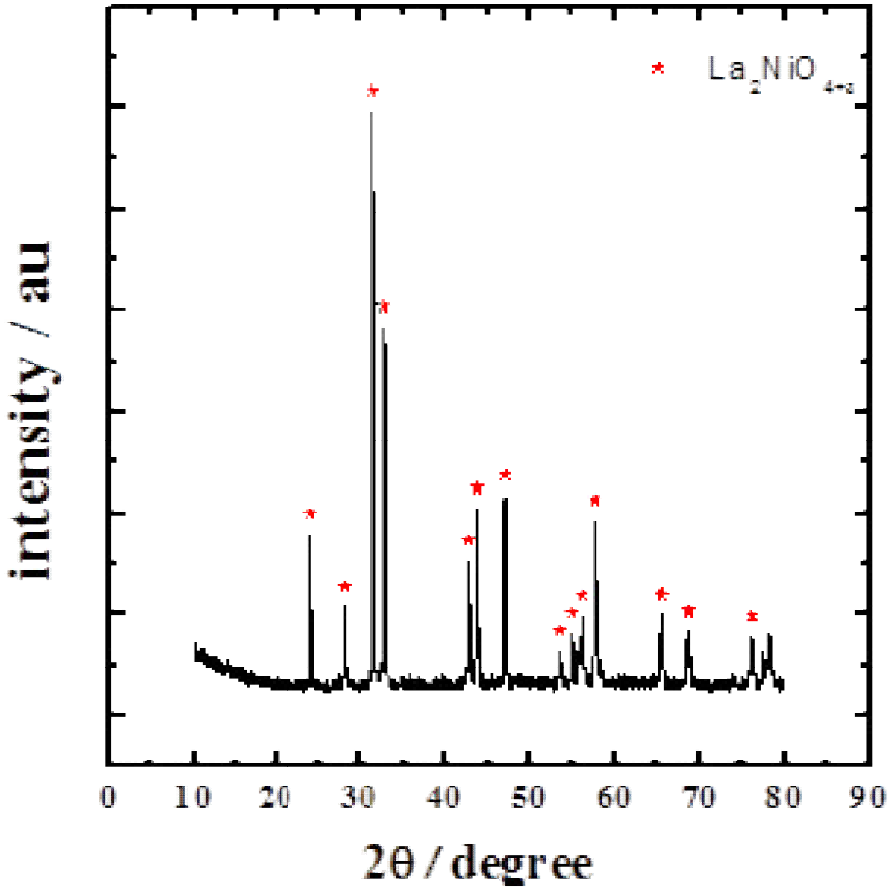

Fig. III.2. X-ray diffraction pattern of undoped $La_2NiO_{4+\delta}$

III.2. Electrochemical Cell Characterization

Thermopowers (θ) of undoped $La_2NiO_{4+\delta}$ are measured with cylinder-shaped specimen with diameter of 11.21±0.03mm and height of 5.29±0.02mm. Fig.III.3 shows schematic of thermocell used for thermopower measurement. YSZs are placed on the top and the bottom of the specimen with S-type thermocouples where they are attached to platinum gauze. Actual views of top, rear, and bottom view of specimen are shown in Fig.III.4 Signals are obtained via two different probes: ionic and electronic probes. Ionic probe signal is gathered from top and bottom of YSZ and electronic probe signal is collected via platinum wires from point-contacted S-type thermocouples embedded inside the specimen. Fig.III.5 shows actual view of point-contacted thermocouple. Notch made on top and bottom of specimen is also shown by using optical microscope. After sealing the $La_2NiO_{4+\delta}$ specimen, temperature gradient is applied to the system by local heater to acquire initial (transient) thermopower and steady state thermopower. Since thermopower measurement requires precise measurement technique, in order to suppress induction effect generated by heater, newly designed heater was used. The schematic and actual views of local heater used are shown in Fig.III.6. After boundary condition is set to be Soret condition, which is the same as Soret equilibrium, thermovoltage signals are obtained from the cell. Ionic and electronic thermovoltage each are expressed as U and V, respectively.

YSZ here is referred to as 8 m/o Y_2O_3-stabilized ZrO_2. For measurement, four individual S-type thermocouples are placed, as shown in Fig.III.3, for temperature measurement. Also, ionic and electronic thermovoltage signals are monitored as well. To meet Soret condition, two different types of glass are applied to the side of the specimen. First, water glass, or sodium silicate-

based glass, is pasted on the surface of the specimen then borosilicate glass is put on the water-glass-sealed sample.

Ionic thermovoltage (U) contains the information of η_i, ionic electrochemical potential, and electronic thermovoltage (V) has η_e, electronic electrochemical potential respectively. For each probes, galvanic cell configuration is expressed as follows.

$$\begin{array}{l} \text{(-) Pt,}a_{O_2} \text{ | YSZ | } La_2NiO_{4+\delta} \text{ | YSZ | } a_{O_2}\text{, Pt (+),} \\ T_{ref} \quad T_4 \quad T_3 \quad T_2 \quad T_1 \quad T_{ref} \end{array} \qquad \text{(III.I)}$$

$$\begin{array}{l} \text{(-) Pt | } La_2NiO_{4+\delta} \text{ | Pt (+)} \\ T_{ref} \quad T_3 \quad T_2 \quad T_{ref} \end{array} \qquad \text{(III.II)}$$

T_1, T_2, T_3, and T_4 each refers to temperature acquired by thermocouple placed on the sample shown in Fig.III.3.1 and T_m is reference temperature which is 0ºC for this experiment. By using this configuration, ionic/electronic electrochemical potential term could be expressed in terms of thermopower (θ).

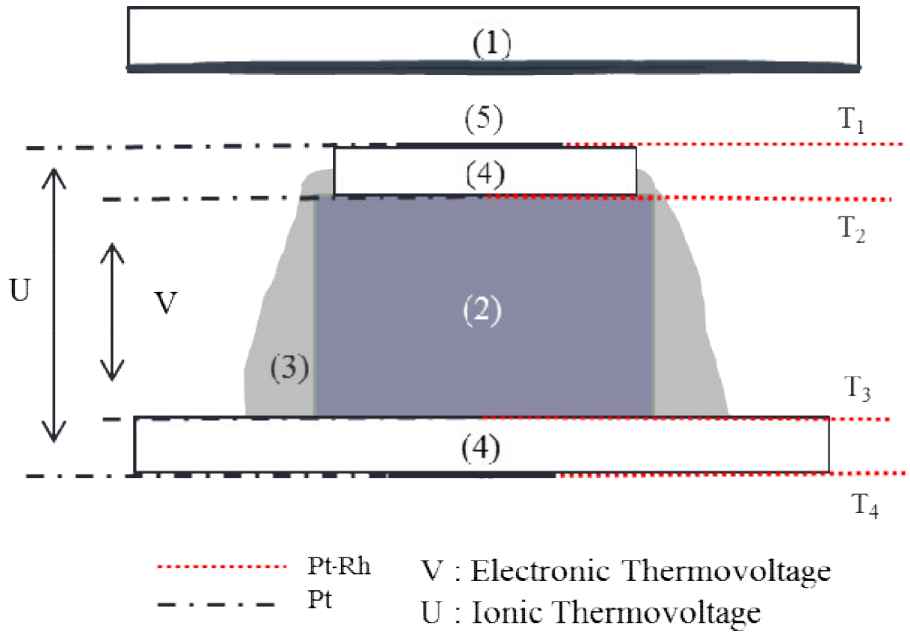

Fig.III.3. The schematic of electrochemical cell for thermopower measurement. (1) Pt–heater; (2) Specimen; (3) Water glass / Borosilicate glass; (4) YSZ plate; (5) Pt-gauze

(a)

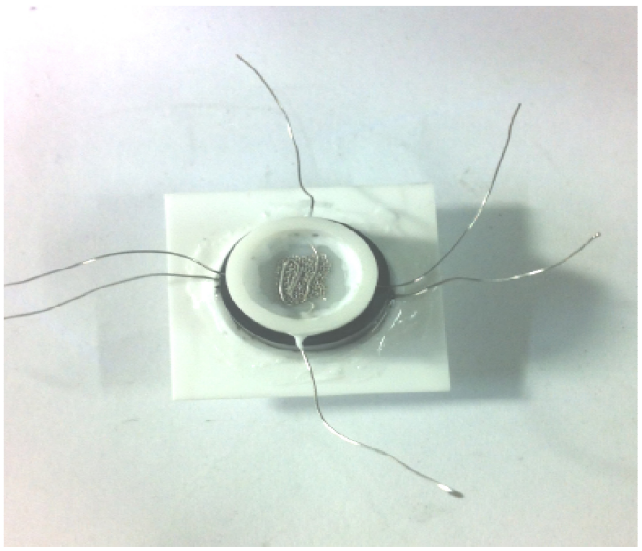

(b)

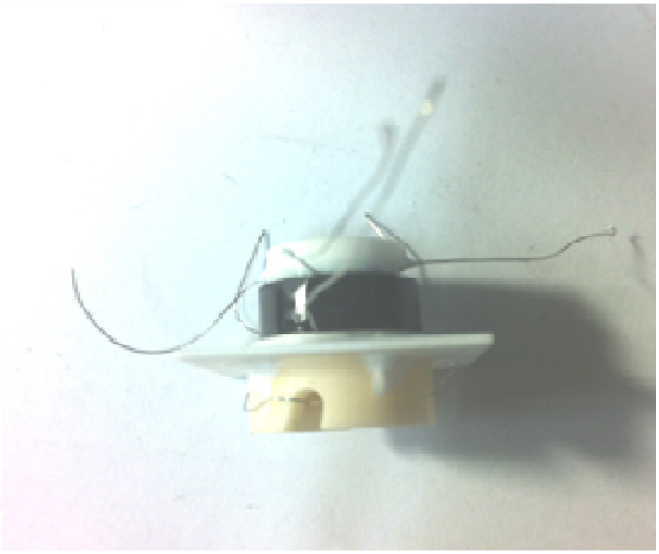

Fig.III.4. Actual view of (a) top, (b) rear, and (c) bottom of specimen obtained via optical microscope.

(c)

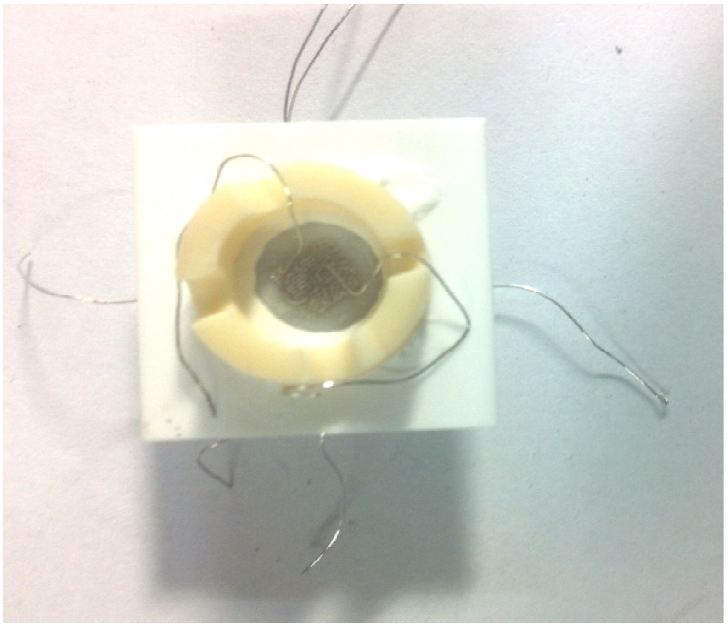

Fig.III.4. (Continued)

(a)

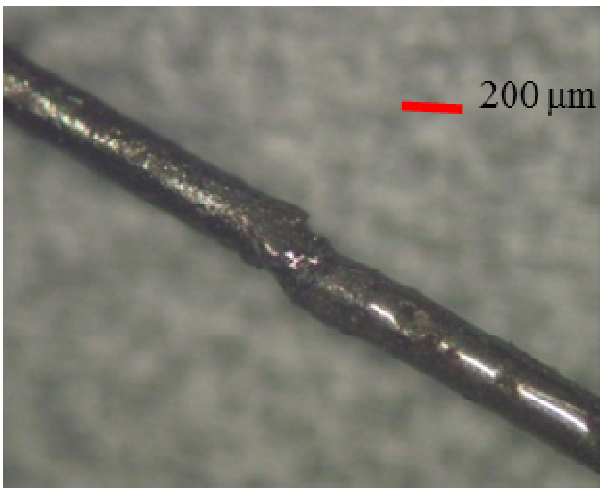

(b)

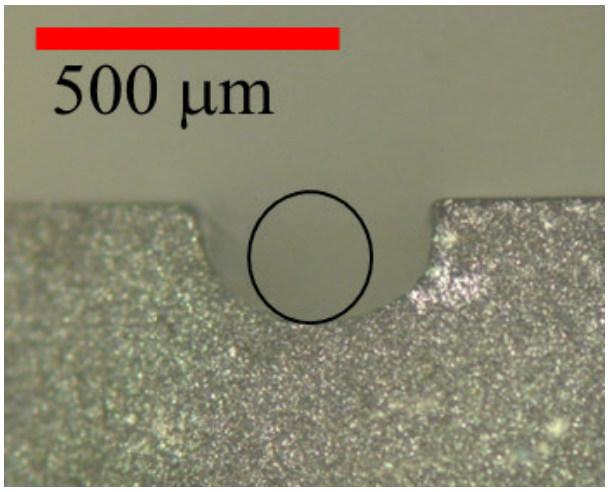

Fig.III.5. (a) Point-contacted S-type thermocouple used in measuring local temperature and electronic thermovoltage. Wire on upper left corner is Pt-Rh wire and one on the bottom right corner is Pt wire. (b) Rear view of notch made on the specimen where circle in the middle represent Pt wire embedded inside, for visual guidance.

(a)

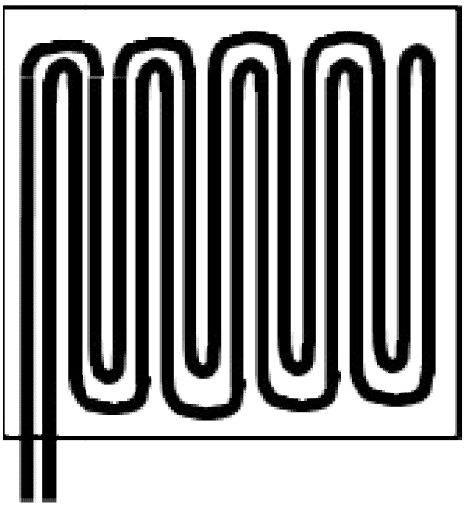

(b)

Fig.III.6. (a) Schematic and (b) actual view of local heater used in experiment. Wire shown in figure is made of platinum where it attached on YSZ plate.

III.3. Sealing Test

As mentioned earlier, boundary condition of the cell is set to be Soret condition and this condition requires condition of closed system. In order to set boundary condition to be Soret condition, it is important to seal specimen from surrounding. For sealing, two different types of glasses are used. After glasses applied to the system, real time change of EMF (U_{21} in Fig III.7) is monitored against oxygen. For this measurement, specimen is equilibrated with outer gas of initial stage ($\log a_{O_2} = -0.67$) by building short circuit between top YSZ. Then specimen's oxygen activity condition is equilibrated with that of reference gas. Then under open circuit condition, oxygen activity of outer gas is changed to $\log a_{O_2} = -0.813 \pm 0.006$. EMF between upper probes (U_{21}) is monitored for 16 hours. Then by using Nernst equation, Eq.(III.1), oxygen activity of specimen is calculated.

$$U_{21} = \frac{RT}{4F} \ln\left(\frac{a_{O_2}^{sp}}{a_{O_2}^{surr}}\right) \qquad \text{(III.1)}$$

In this equation, U_{21}, $a_{O_2}^{sp}$, and $a_{O_2}^{ref}$ refer to EMF of upper probe, oxygen activity of specimen, and oxygen activity of surrounding gas. The result is shown in Fig.III.8. It is shown that for time, oxygen activity of specimen stays constant although surrounding's oxygen activity varies. So, it can be concluded that specimen is in closed system and Soret condition can be assumed for further experiment.

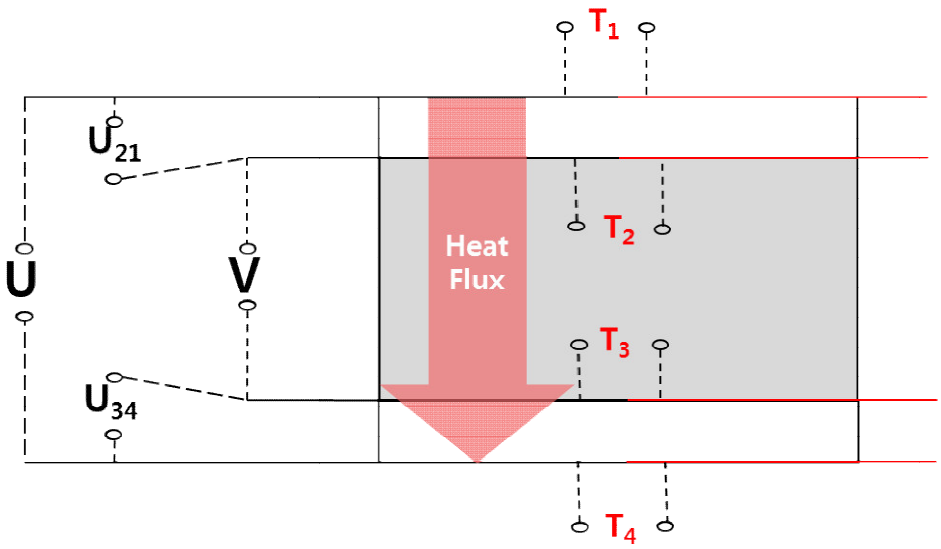

$$\Delta T' = T_1 - T_4 \; ; \; \Delta T = T_2 - T_3$$

Fig.III.7. All raw information contents acquired from 2-probe thermoelectric cell where (1) YSZ, (2) LNO specimen, and (3) YSZ. For temperature measurement, black lines refer to platinum wire and red lines refer to Pt-Rh wire. Cell design is the same as Fig.III.3.1 where this figure concentrate on actual signals retrieved off the cell.

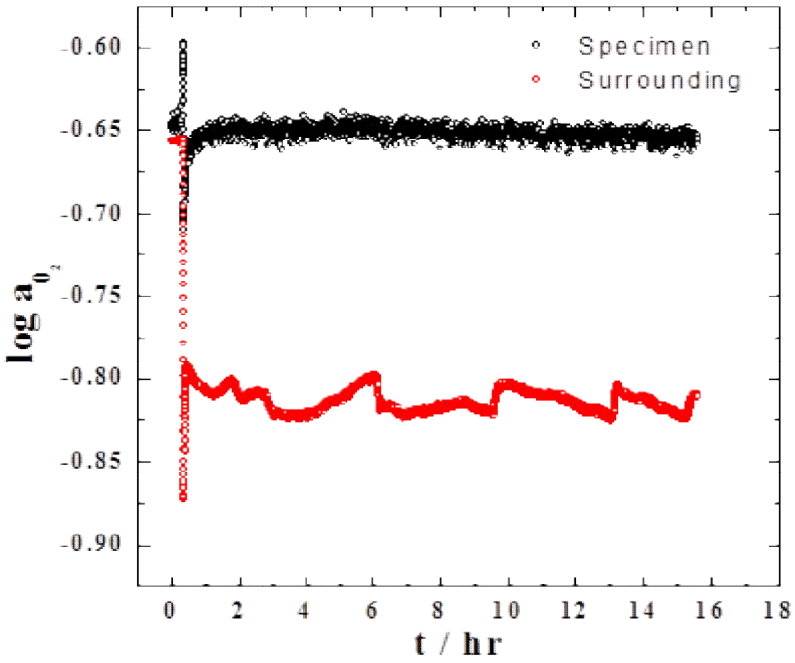

Fig.III.8. Variation of oxygen activity of specimen against time after changing surrounding oxygen activity. (Sealing test results)

III.4. Thermopower (θ) measurement and Calculation

In this experiment, thermodynamic condition of cell is controlled in three individual temperatures 1000ºC, 900ºC, and 800ºC with oxygen activity range of $-6 < \log a_{o_2} < -0.67$. For $-3.5 < \log a_{O_2} < -0.67$, oxygen activity of specimen is equilibrated with that of surrounding gas before measurement. For $\log a_{O_2} < -4$, oxygen activity of surrounding is set to be $\log a_{O_2} \sim -4$ and oxygen ion is pumped in or pumped out by using YSZ in Fig.III.3. Oxygen activity of surrounding is controlled by mixing oxygen gas and other inert gas.

For glasses, two different types of glasses, borosilicate glass and water glass, are applied to the side of specimen. Then by using local heater, temperature gradient is generated. From Pt lead wire between T_2 and T_3 from Fig.III.3 electronic thermovoltage (V) was obtained and from Pt wire from T_1 and T_4 thermocouple, ionic thermovoltage (U) was acquired for raw signal. As mentioned in Fig.III.3, $\Delta T'$ and ΔT each represents $\Delta T' = T_1 - T_4$, $\Delta T = T_2 - T_3$. Galvanic cell configuration is given for ionic signal (III.I) and for electronic signal (III.II). Electronic thermovoltage here contains information contents as follows:

$$V = \frac{\Delta \eta_e}{F} - \int_{T_2}^{T_3} \theta^{Pt} dT \qquad \text{(III.2)}$$

For ionic thermovoltage, signal obtained means as follows:

$$U = -\frac{\Delta(\eta_i - \mu_o^{ref})}{F} - \int_{T_1}^{T_4} \theta^{Pt} dT + \theta^{YSZ}(\Delta T' - \Delta T) \qquad \text{(III.3)}$$

$\mu_{\mathrm{o}}^{\mathrm{ref}}$, θ^{Pt}, and θ^{YSZ} here represent chemical potential of reversible ionic probe which exposed to reference gas, thermopower of platinum, and thermopower of YSZ, respectively. For thermopower of platinum and YSZ, data from previous studies are used [40, 41].

Eq. (III.2) and (III.3) can be obtained from following procedure. From Fig.III.9, signal U basically consist of electrochemical potential difference of hole.

$$\mathrm{F}U = \eta_{\mathrm{e,mu}}(\mathrm{T_{ref}}) - \eta_{\mathrm{e,md}}(\mathrm{T_{ref}}) \tag{III.4}$$

Then by adding and subtracting actual data coming out from specimen,

$$\mathrm{F}U = \eta_{\mathrm{e,mu}}(\mathrm{T_{ref}}) - \eta_{\mathrm{e,l}}(T_1) + \eta_{\mathrm{e,l}}(T_1) - \eta_{\mathrm{e,2}}(T_2) + \eta_{\mathrm{e,2}}(T_2) - \eta_{\mathrm{e,md}}(\mathrm{T_{ref}}), \tag{III.5}$$

Eq. (III.5) can be obtained. Thermopower of platinum wire [41] and YSZ [40] can be written as follows.

$$\theta^{\mathrm{Pt}} = \frac{1}{\mathrm{F}}\frac{\mathrm{d}\eta_{\mathrm{e}}}{\mathrm{d}T} \tag{III.6}$$

$$\theta^{\mathrm{YSZ}} = -\frac{1}{\mathrm{F}}\frac{\mathrm{d}\eta_{\mathrm{e}}}{\mathrm{d}T} \tag{III.7}$$

Then, Eq. (III.5) can be transformed into Eq. (III.8)

$$\mathrm{FU} = \eta_{\mathrm{e},1}(\mathrm{T}_1) - \eta_{\mathrm{e},4}(\mathrm{T}_4) - \mathrm{F}\int_{\mathrm{T}_1}^{\mathrm{T}_4} \theta^{\mathrm{Pt}}\mathrm{dT} \tag{III.8}$$

And thermovoltage induced between ionic probes can be written as follow.

$$\theta^{\mathrm{YSZ}}(T_1 - T_2) = \int_{\mathrm{T}_2}^{\mathrm{T}_1} \theta^{\mathrm{YSZ}}\mathrm{dT} = \frac{1}{\mathrm{F}}\int_{\mathrm{T}_2}^{\mathrm{T}_1} \frac{\mathrm{d}\eta_{\mathrm{e}}}{\mathrm{d}T}\mathrm{d}T = \frac{1}{\mathrm{F}}[\eta_{\mathrm{e},1} - \eta_{\mathrm{e},2}] \tag{III.9(a))}$$

$$\theta^{\mathrm{YSZ}}(T_3 - T_4) = \int_{\mathrm{T}_4}^{\mathrm{T}_3} \theta^{\mathrm{YSZ}}\mathrm{dT} = \frac{1}{\mathrm{F}}\int_{\mathrm{T}_4}^{\mathrm{T}_3} \frac{\mathrm{d}\eta_{\mathrm{e}}}{\mathrm{dT}}\mathrm{dT} = \frac{1}{\mathrm{F}}[\eta_{\mathrm{e},3} - \eta_{\mathrm{e},4}] \tag{III.9(b))}$$

Also Eq. (III.8) can also be written as:

$$\begin{aligned} \mathrm{F}U = {} & \eta_{\mathrm{e},1}(T_1) - \eta_{\mathrm{e},2}(T_2) + \eta_{\mathrm{e},2}(T_2) - \eta_{\mathrm{e},3}(T_3) \\ & + \eta_{\mathrm{e},3}(T_3) - \eta_{\mathrm{e},4}(T_4) - \mathrm{F}\int_{\mathrm{T}_1}^{\mathrm{T}_4} \theta^{\mathrm{Pt}}\mathrm{dT} \end{aligned} \tag{III.10}$$

With Eq. (III.9(a)) and (III.9(b)), Eq. (III.10) changes into:

$$\mathrm{F}U = \eta_{\mathrm{e},2}(T_2) - \eta_{\mathrm{e},3}(T_3) + \mathrm{F}\theta^{\mathrm{YSZ}}(T_1 - T_2) + \theta^{\mathrm{YSZ}}(T_3 - T_4) - \mathrm{F}\int_{\mathrm{T}_1}^{\mathrm{T}_4} \theta^{\mathrm{Pt}}\mathrm{dT} \tag{III.11}$$

Then with Eq. (II.46), Eq. (III.11) is written as:

$$\mathrm{F}U = \frac{1}{2}\left[\mu_{\mathrm{O},2}(\mathrm{a}_{\mathrm{O}_2}, T_2) - \eta_{\mathrm{i},2}(T_2)\right] - \frac{1}{2}\left[\mu_{\mathrm{O},3}(a_{\mathrm{O}_2}, T_3) - \eta_{\mathrm{i},3}(T_3)\right] + \mathrm{F}\theta^{\mathrm{YSZ}}(T_1 - T_2) + \theta^{\mathrm{YSZ}}(T_3 - T_4) - \mathrm{F}\int_{\mathrm{T_1}}^{\mathrm{T_4}} \theta^{\mathrm{Pt}}\mathrm{dT} \quad \text{(III.12)}$$

Finally, Eq. (III.3) can be obtained. The same procedure is done for electronic thermovoltage.

By rephrasing Eq. (III.2) and Eq. (III.3),

$$\frac{\Delta\eta_{\mathrm{e}}}{\mathrm{F}} = V + \int_{\mathrm{T_2}}^{\mathrm{T_3}} \theta^{\mathrm{Pt}}\mathrm{dT} \quad \text{(III.13)}$$

$$-\frac{\Delta(\eta_{\mathrm{i}} - \mu_{\mathrm{o}}^{\mathrm{ref}})}{\mathrm{F}} = U + \int_{\mathrm{T_1}}^{\mathrm{T_4}} \theta^{\mathrm{Pt}}\mathrm{dT} - \theta^{\mathrm{YSZ}}(\Delta T' - \Delta T) \quad \text{(III.14)}$$

Thermopower of platinum and that of YSZ does not depend on time but only depend on temperature applied [40]. So, Eq.(III.13) and Eq.(III.14) can be modified after using definition of thermopower Eq.(III.15).

$$\lim_{\Delta \mathrm{T} \to 0}\left(-\frac{1}{\mathrm{F}}\frac{\Delta\eta_{\mathrm{e}}}{\Delta T}\right) = \theta_{\mathrm{e}} \quad \text{(III.15)}$$

$$\lim_{\Delta T \to 0}\left[-\frac{1}{2\mathrm{F}}\frac{\Delta\left(\eta_i - \mu_o^{ref}\right)}{\Delta T}\right] = \theta_{\mathrm{i}} - \frac{1}{2\mathrm{F}}S_{\mathrm{o}}^{\mathrm{ref}} \quad \text{(III.16)}$$

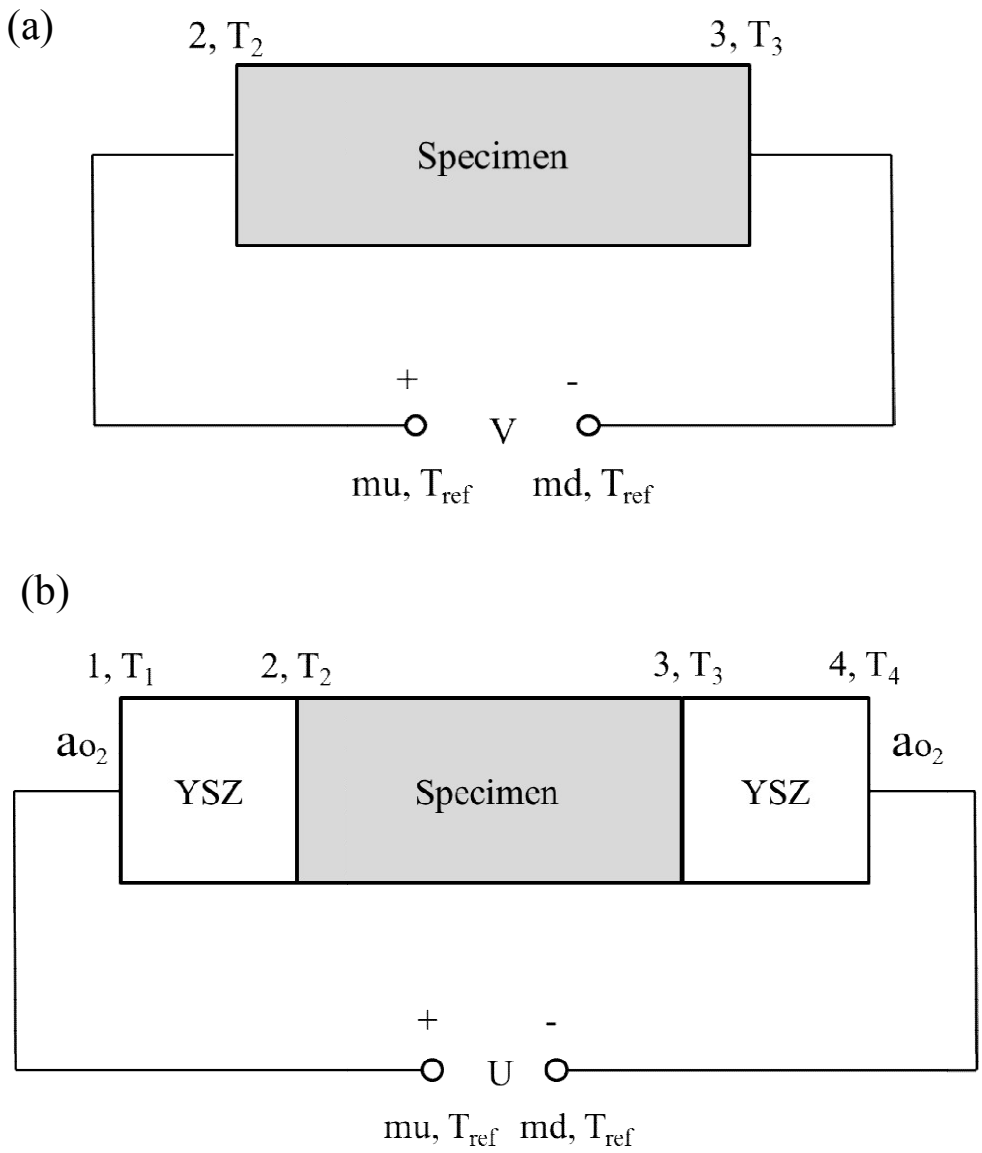

Fig.III.9. Schematic of galvanic cell configuration of obtaining electronic thermovoltage, V, and ionic thermovoltage, U. For each position, two letters separated by comma each represents the name of position and temperature at that position, respectively.

Here, S_o^{ref} is entropy of reference gas. By removing S_o^{ref} from Eq.(III.16), ionic thermopower can be obtained. S_o^{ref} is written in function as follows:

$$S_o^{ref} = \frac{1}{2} S_{O_2,g}^o - \frac{R}{2} \ln a_{O_2}^{ref} \tag{III.17}$$

$S_{O_2,g}^o$ and $a_{O_2}^{ref}$ each refers to standard oxygen entropy and oxygen activity, respectively. $a_{O_2}^{ref}$ can be obtained from oxygen sensor directly in real time. From previous studies, the value of $S_{O_2,g}^o$ is written in function of temperature as follows [42]:

$$\begin{aligned} S_{O_2,g}^o / \mathrm{JK^{-1}mol^{-1}} \\ = R\left[-\frac{n_1}{1.5} T^{-1.5} + n_2 \ln T + \frac{n_3}{2} T^2 + n_4 \left\{ \frac{u e^u}{e^u - 1} - \ln(e^u - 1) \right\} \right. \\ \left. + n_5 \left\{ \frac{\frac{2}{3}\eta e^{-\eta}}{1 + \frac{2}{3} e^{-\eta}} + \ln\left(1 + \frac{2}{3} e^{-\eta}\right) \right\} - \ln\left(\frac{P}{P_a}\right) \right]_{298.15k}^{t} + 205.037 \end{aligned} \tag{III.18}$$

Here, $u = n_6 / T$, $\eta = n_7 / T$, and $P_a = 0.1$Mpa. P stands for standard pressure. Standard pressure was set to be 1 atm (P=0.101325MPa). Lastly entropy difference of oxygen from 0K to 298.15K was added. Constant values used in Eq. (III.18) are shown below in Table.III.1.

Table.III.1. Numerical values of the coefficient n_i of Eq. (III.19) [41]

$\mathbf{n_1}$	1.06778
$\mathbf{n_2}$	3.50042
$\mathbf{n_3}$	0.116961e-7
$\mathbf{n_4}$	1.01258
$\mathbf{n_5}$	0.944365
$\mathbf{n_6}$	2242.45K
$\mathbf{n_7}$	11580.4K

IV. Results/Analyses

Soret experiment is defined as experiment performed under temperature gradient upon closed system. Since specimen is separated with outer surrounding, it can be assumed that system is in the state of close system. By applying current on local heater as shown in Fig.III.3, local temperature gradient is applied to the system. After heating up upper part of this thermoelectric cell, heat flux is generated from top to bottom of the system. Under this condition, U, V, $\Delta T'$, and ΔT are monitored with respect to time and plotted at Fig.IV.1, and Fig.IV.2.

IV.1. Thermoelectric property of $La_2NiO_{4+\delta}$ under Soret Condition

From this thermoelectric cell, U, V, $\Delta T'$, and ΔT signals are obtained and plotted against time in Fig.IV.1 and Fig.IV.2. By looking into Fig.IV.1, it can be intuitively visualized that electronic thermovoltage and ionic thermovoltage signals shows different behavior. Electronic thermovoltage signal (V, Fig.IV.1(a)) polarizes to one side after heater is turned on while ionic thermovoltage signal (U, Fig.IV.1(b)) increases after signal decreases in first hand. After removing signals embedded in original signal (thermovoltage platinum and YSZ), only $\Delta\eta_e/F$ and $-\Delta(\eta_i-\mu_o^{ref})/F$ are left. $\Delta\eta_e/F$ and $-\Delta(\eta_i-\mu_o^{ref})/F$ against time are plotted in Fig.IV.3. The same as ionic thermovoltage signal, $-\Delta(\eta_i-\mu_o^{ref})/F$ also shows behavior where increase in signal occurs followed by initial decrease in signal as shown in Fig.IV.3(b). This behavior occur due to effect generated by $\Delta\mu_o^{ref}/F$ is dominant initially then signal variation due to chemical polarization result in increase in value of $-\Delta(\eta_i-\mu_o^{ref})/F$.

Meanwhile, in Fig.IV.4, by using time as parameter, $\Delta\eta_e/F$ and $-\Delta(\eta_i-\mu_o^{ref})/F$ from Fig.IV.3(a) and Fig.IV.3(b) are plotted with respect to ΔT. In Fig.IV.4, $-\Delta(\eta_i-\mu_o^{ref})/F$ varies linearly against temperature when heater is turned on or turned off. But linearity behavior does not vividly show on $\Delta\eta_h/F$. Behavior of $-\Delta(\eta_i-\mu_o^{ref})/F$ can be explained with Eq. (II.56) and Eq. (II.57). For initial stage of heating before chemical polarization occur, $\nabla\delta=0$ that $(\partial\mu_o/\partial\delta)_T\nabla\delta$ term can be assume to be zero. After short period of time, chemical polarization can be observed that $(\partial\mu_o/\partial\delta)_T\nabla\delta$ cannot be neglected. So, latter polarization is governed by $(\partial\mu_o/\partial\delta)_T\nabla\delta$ term. For comparison of heating and cooling process, initial behavior of signal should

be identical. In other words, initial variation of signal with respect to temperature alteration should be the same. This can only be assumed under condition when relatively small temperature difference is applied to the system. With that assumption, specimen's transport properties can be assumed to be constant [27]. Maximum temperature variance between top and bottom of specimen is set to be approximately 7K that symmetrical shape of signal is obtained that assumption could be validly used.

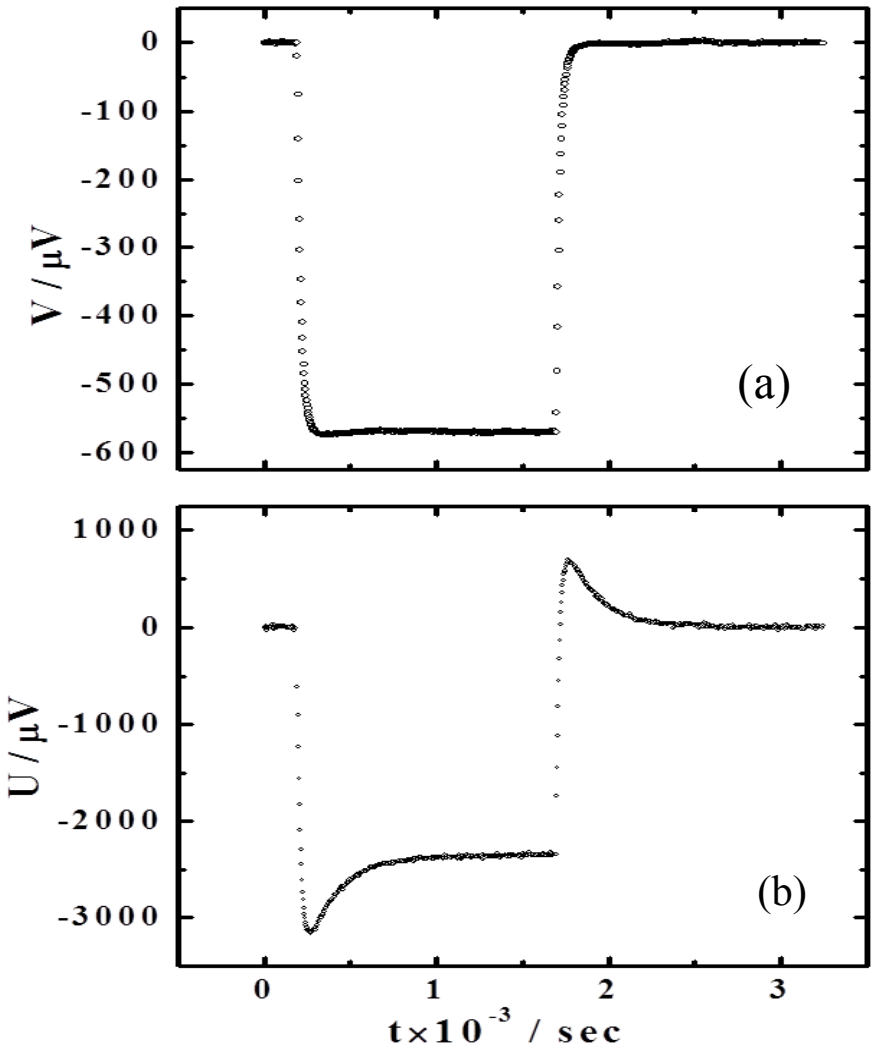

Fig.IV.1. Typical temporal variation of (a) V, (b) U during heating (heater-on) and subsequent cooling (heater-off) at 1000ºC in $\log a_{O_2} = \log a_{O_2}^{ref} = -1.985 \pm 0.001$.

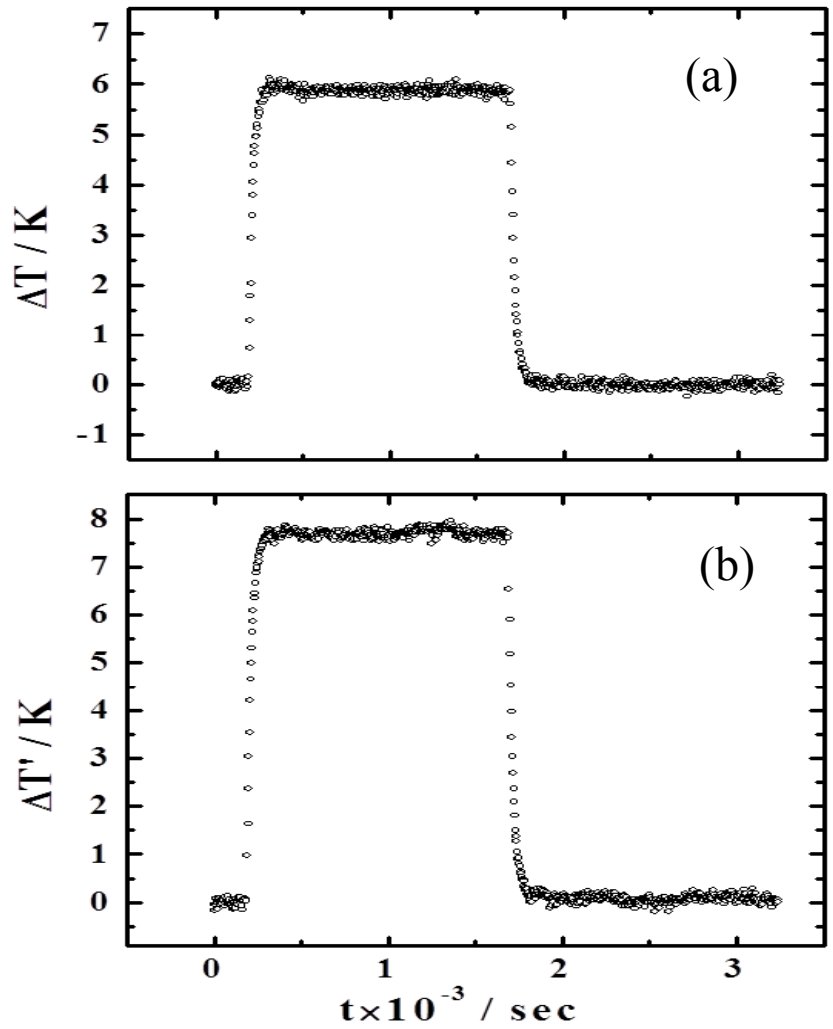

Fig.IV.2. Typical temporal variation of (a) ΔT, (b) ΔT′ during heating (heater-on) and subsequent cooling (heater-off) at 1000ºC in $\log a_{O_2} = \log a_{O_2}^{ref}$ = -1.985±0.001. Here $\Delta T' = T_1 - T_4$; $\Delta T = T_2 - T_3$

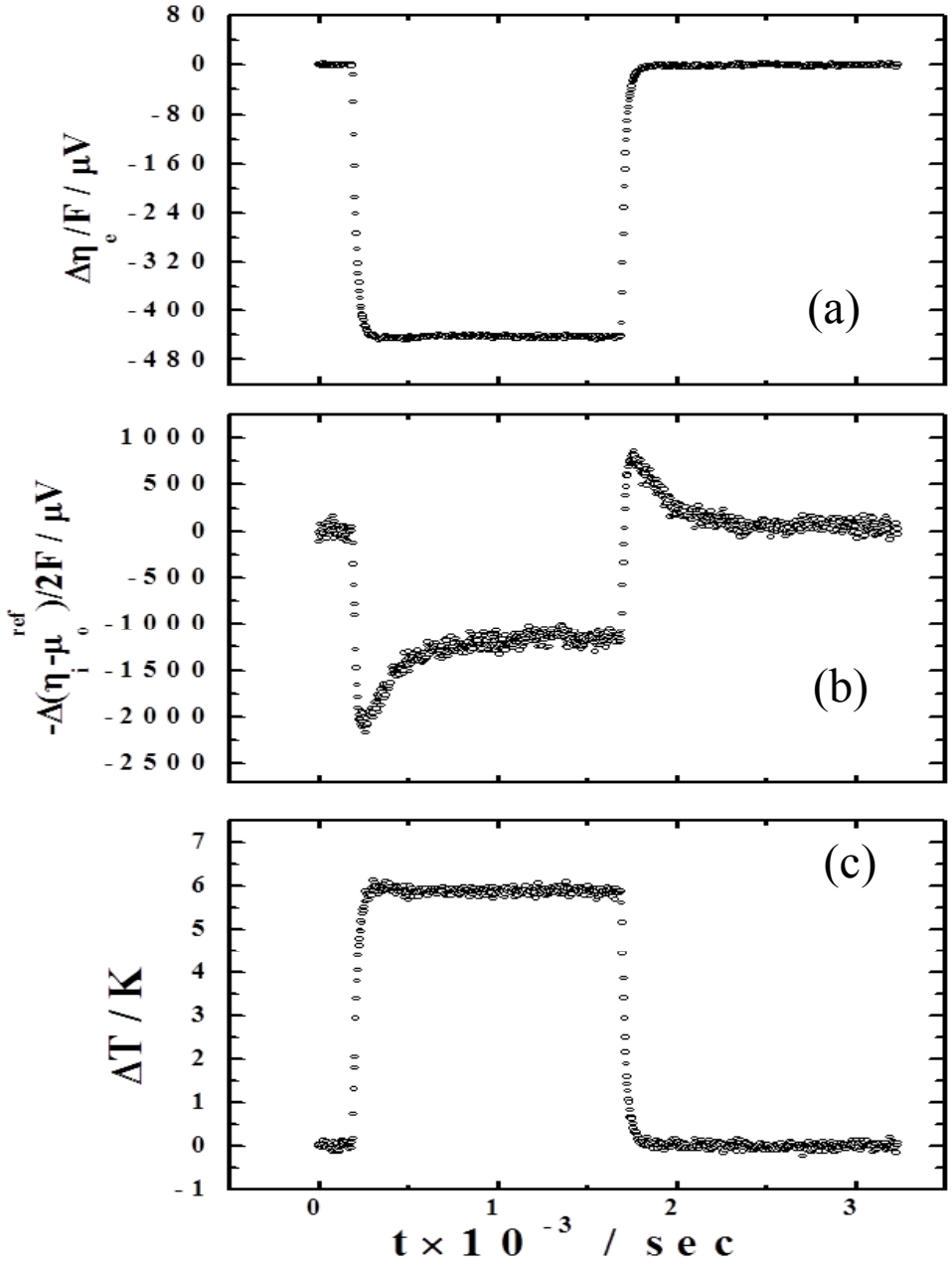

Fig.IV.3. Typical temporal variation of (a) $\Delta\eta_e/F$, (b) $-\Delta(\eta_i-\mu_o^{ref})/F$, and (c) ΔT during heating (heater-on) and subsequent cooling (heater-off) at1000ºC in $\log a_{O_2} = \log a_{O_2}^{ref}$ = -1.985±0.001. Where $\Delta T = T_2-T_3$.

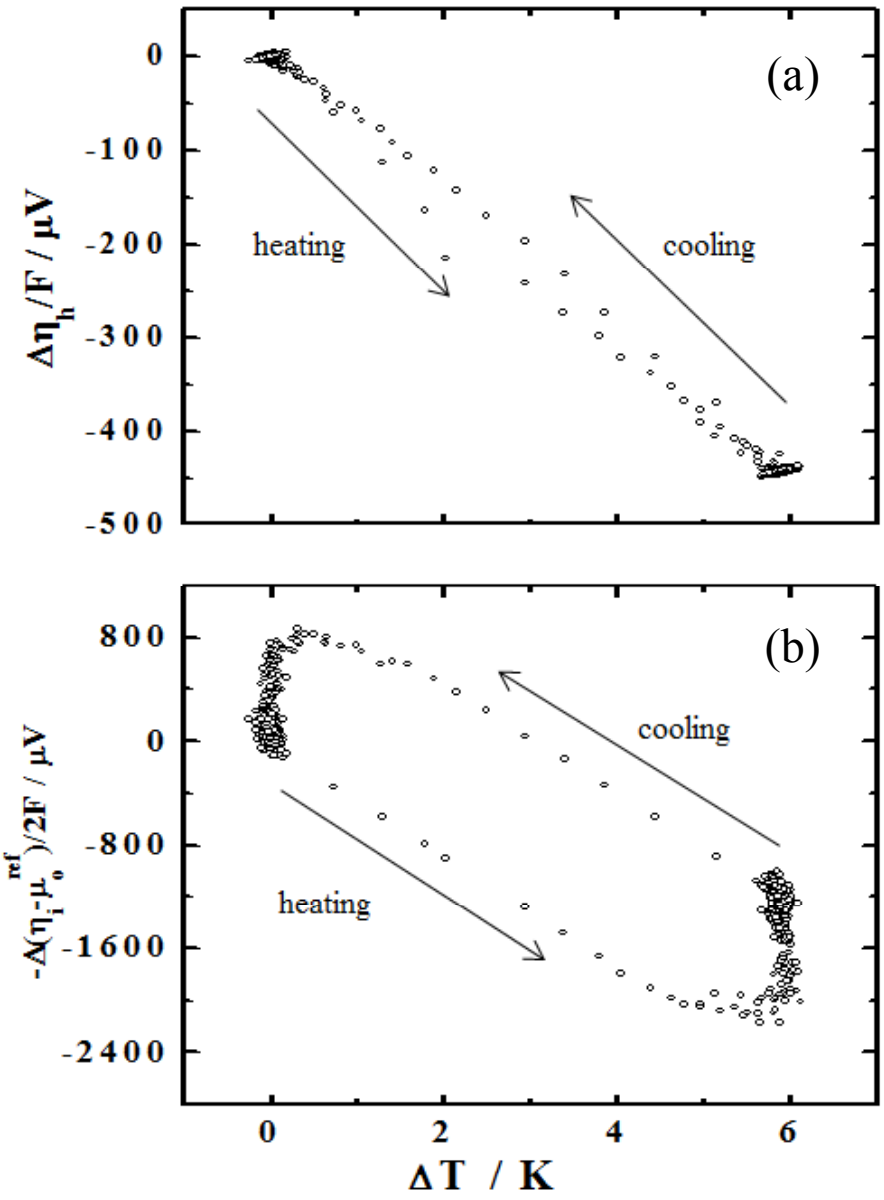

Fig.IV.4. Behavior of (a) $\Delta\eta_e/F$, (b) $-\Delta(\eta_i-\mu_o^{ref})/F$ with respect to ΔT during heating (heater-on) and subsequent cooling (heater-off) at1000ºC in $\log a_{O_2}$ = $\log a_{O_2}^{ref}$ = -1.985±0.001. Where $\Delta T = T_2-T_3$.

Ionic and electronic thermopower under Soret equilibrium can be obtained from following analysis. By averaging out initial and steady state values from Fig.IV.3(a) and Fig.IV.3(b) as well as the temperature difference at this condition. As shown in Fig.IV.5, for different temperature gradients are applied to system and steady state thermopowers under Soret condition are obtained. Fig.IV.5 continuously showing representative data under condition of temperature condition of 1000ºC in $\log a_{O_2} = \log a_{O_2}^{ref} = -1.985 \pm 0.001$. Four different temperature gradients are applied to the system that linear regression is performed in order to obtain slope for ionic and electronic partial thermopower. θ_h^{st}, partial electronic thermopower, and $\theta_i^{st} - S_o^{ref}/2F$, partial ionic thermopower with reference oxygen entropy, are obtained by calculating slope of $\Delta\eta_h/F$ and $-\Delta(\eta_i - \mu_o^{ref})/F$ with respect to ΔT, where $\Delta T = T_2 - T_3$. For partial ionic thermopower acquisition, term $S_o^{ref}/2F$ should be revised by using Eq. (II.17) and Eq. (II.18). After revision, partial ionic thermopower, θ_i^{st}, is obtained. Those two individual partial thermopowers are plotted on Fig.IV. 6.

It can be noted that under Soret equilibrium, partial electronic thermopower and partial ionic thermopower each has negative and positive values, respectively. Also, partial ionic thermopower's variation against oxygen activity seems to increase as temperature decreases.

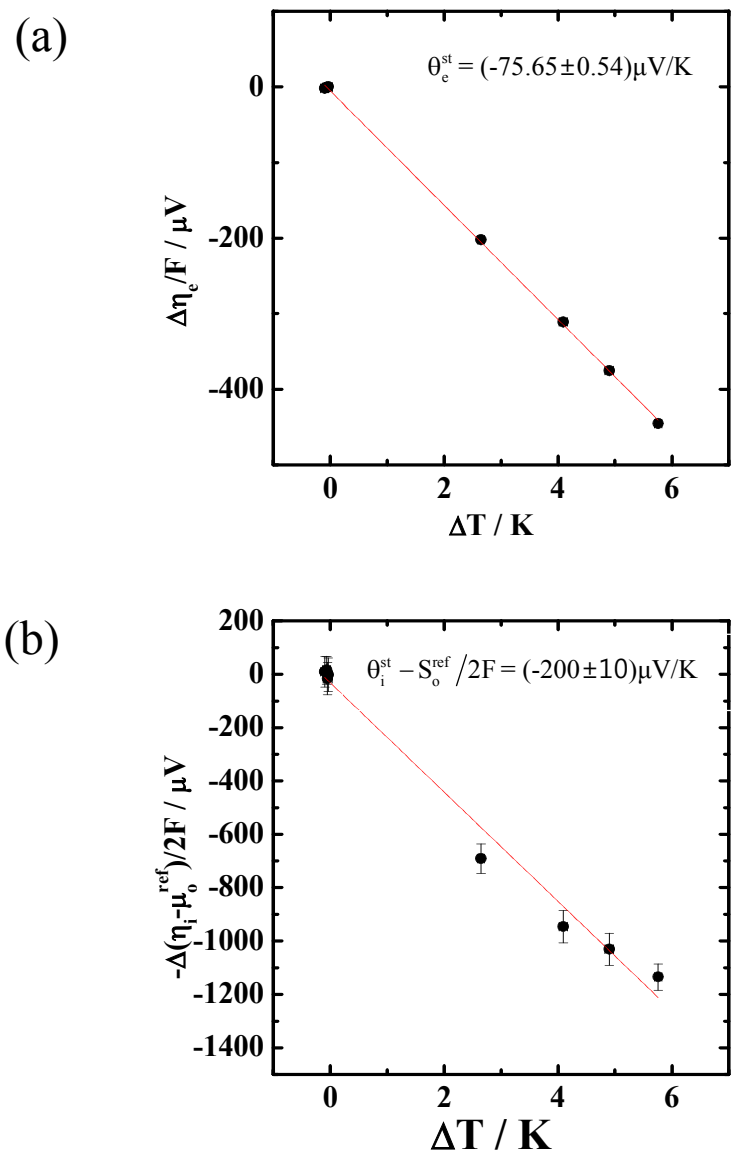

Fig.IV.5. (a) $\Delta\eta_e/F$ and (b) $-\Delta(\eta_i-\mu_o^{ref})/F$ under Soret equilibrium with respect to at1000ºC in $\log a_{O_2} = \log a_{O_2}^{ref}$ = -1.985±0.001. Slope obtained from here indicates θ_e^{st} for (a) and $\theta_i^{st} - S_o^{ref}/2F$ for (b) where $\Delta T = T_2 - T_3$.

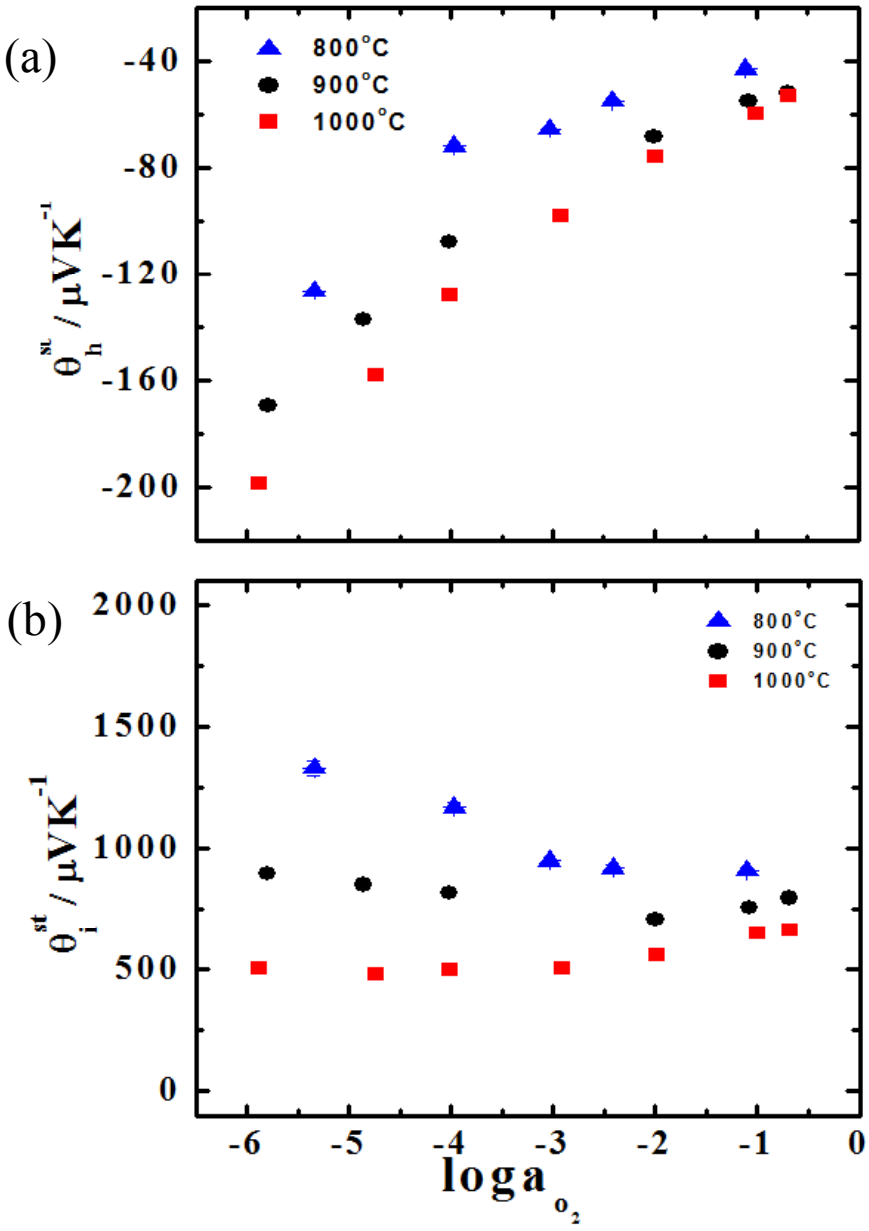

Fig.IV.6. (a) partial electronic thermopower under Soret condition, θ_i^{st}, and (b) partial electronic thermopower, θ_e^{st}, vs. $\log a_{O_2}$ at 1000ºC, 900ºC, and 800ºC.

As mentioned earlier, two non-isothermal transport coefficients, L_{iT} and L_{eT}, are in the form of isothermal transport coefficients and partial ionic and electronic thermopower under Soret condition as shown in Eq.(II.45). Then by obtained steady state thermopower values, non-isothermal transport coefficient is calculated. Isothermal transport coefficients for $La_2NiO_{4+\delta}$ data are obtained from previous study shown in Fig.IV.7 [21]. By using Eq.(II.45), non-isothermal transport coefficients are calculated and plotted in Fig.IV.8. Since non-isothermal transport coefficients are positive in values, it can be concluded that if there is no direct driving force ($\nabla\eta_i$, $\nabla\eta_e$) for ion and hole but only temperature gradient (∇T) works as a driving force, both hole and ion moves from hot spot to cold area.

Interesting phenomena are obsereved from this analysis. Intuitively, non-isothermal transport coefficients should be decreased against temperature. Data, however, shows non-isothermal tranport coeffcients stays almost constant within error range. Reason of this phenomena is yet to be evaluated.

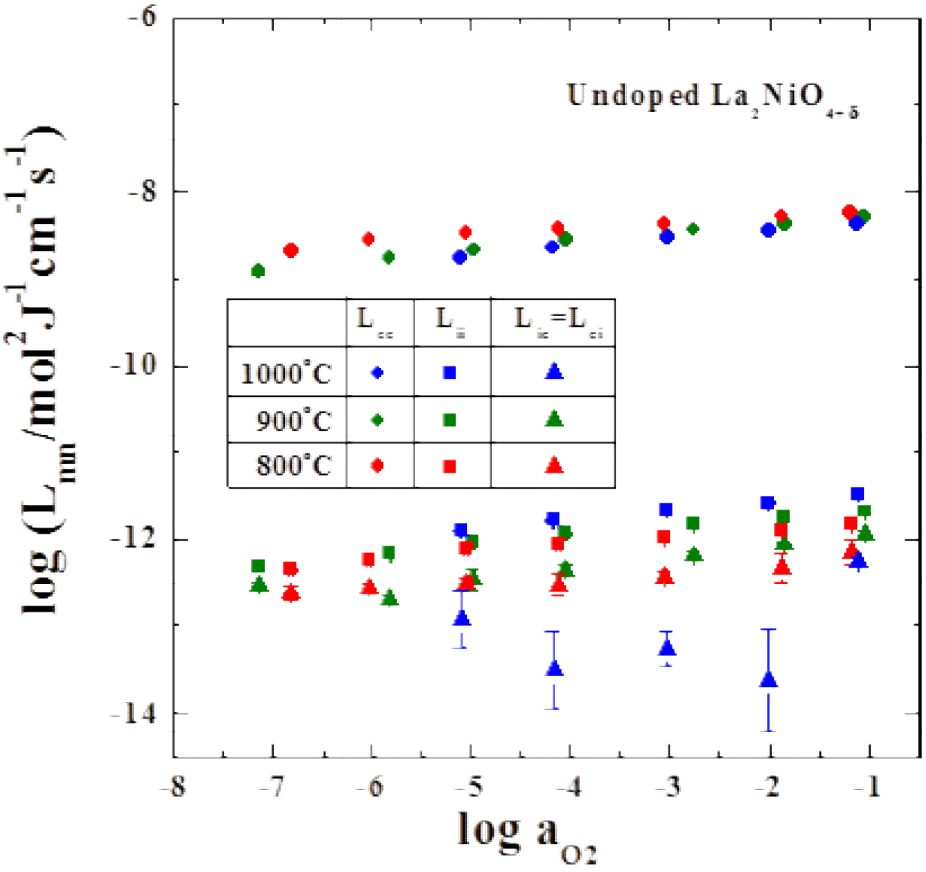

Fig.IV.7. Isothermal Onsager transport coefficients vs. oxygen activity of $La_2NiO_{4+\delta}$ [21].

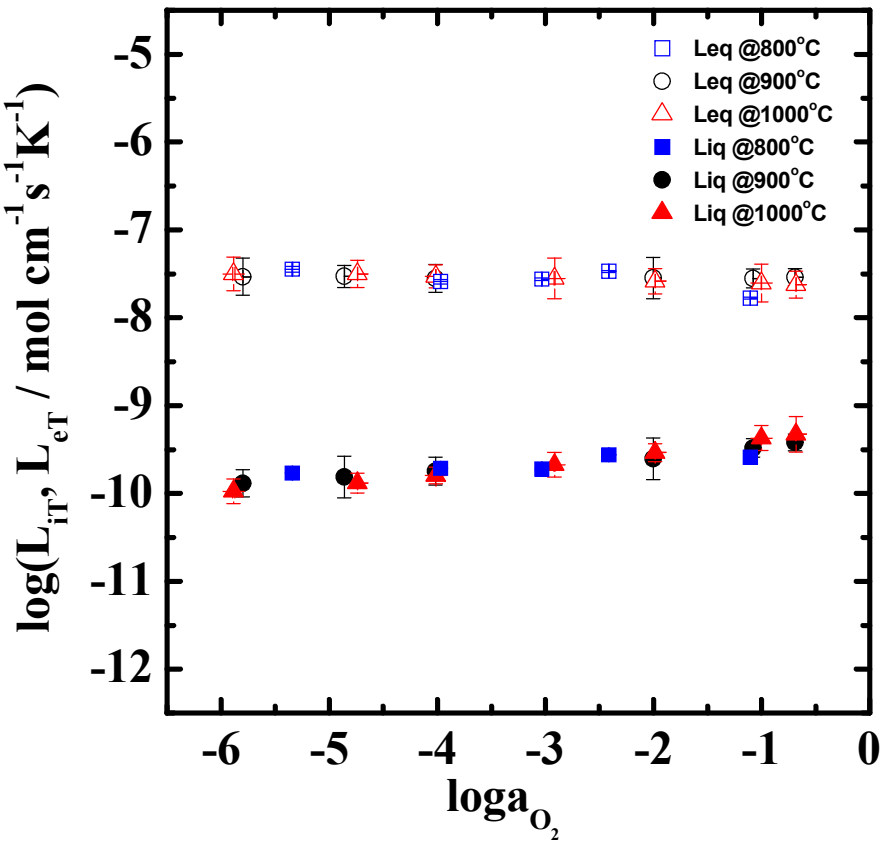

Fig.IV.8. Non-isothermal Onsager transport coefficients vs. oxygen activity of $La_2NiO_{4+\delta}$

By understanding temperature gradient applied to the system equivalently works as a concentration gradient; effect of temperature gradient upon oxygen activity has been studied [23]. Using 2x3 transport coefficient matrix, Eq. (II.24), with open circuit condition, $\sum_{k=i,e} z_k F J_k = 0$, and equilibrium reaction, $\nabla\mu_o = \nabla\eta_i + 2\nabla\eta_e ; O \leftrightarrow O^{2-} + 2h^+$, flux of oxygen ion is expressed as that of oxygen atom. Equation is as follows.

$$J_o = J_i = -L_{ii}\left[1 - t_i\left(1 - \frac{L_{ie}}{2L_{ii}}\right)\right]\nabla\mu_o + \left[\left(2L_{ii} - L_{ie}\right)f - L_{iT}\right]\nabla T \qquad \text{(IV.1(a))}$$

$$= -L_{ii}\left[1 - t_i\left(1 - \frac{L_{ie}}{2L_{ii}}\right)\right]\left(\nabla\mu_o + \bar{\bar{S}}_o\nabla T\right) \qquad \text{(IV.1(b))}$$

To separate oxygen flux according to driving force, flux can be separated in two different parts, J_o^{chem} and J_o^{Therm}. Here, J_o^{chem} is flux induced by oxygen's chemical potential where J_o^{Therm} is flux generated by using temperature gradient. Those terms can be expressed as, $J_o^{chem} = -L_{ii}\left[1 - t_i\left(1 - \frac{L_{ih}}{2L_{ii}}\right)\right]\nabla\mu_o$ and $J_o^{Therm} = \left[\left(2L_{ii} - L_{ie}\right)f - L_{iT}\right]\nabla T$. To understand effect of temperature gradient on chemical potential gradient, it is assumed that $J_o^{chem} = J_o^{Therm}$. Under this relation, between chemical potential gradient and temperature gradient, following relation can be expressed:

$$\frac{\nabla\mu_o}{\nabla T} \approx \frac{\Delta\mu_o}{\Delta T} = \bar{\bar{S}}_o \qquad \text{(IV.2)}$$

By changing chemical potential difference into oxygen activity difference, following equation is obtained.

$$\frac{\Delta \log a_{o_2}}{\Delta T} = \frac{2}{2.303RT} \overline{\overline{S}}_o \qquad \text{(IV.3)}$$

Then, by using Eq. (II.70) and Eq. (II.71), Eq. (IV.3) can be transformed into Eq. (IV.4)

$$\frac{\Delta \log a_{o_2}}{\Delta T} = \frac{4F\left(\theta_i^{st} - \theta_e^{st}\right)}{2.303RT} \qquad \text{(IV.4)}$$

Then effect of temperature gradient against oxygen activity is plotted in Fig.IV.9. It can be concluded that oxygen permeation amount generated by 200 ~ 300K temperature difference within specimen is equivalent to that of 10 times of oxygen activity.

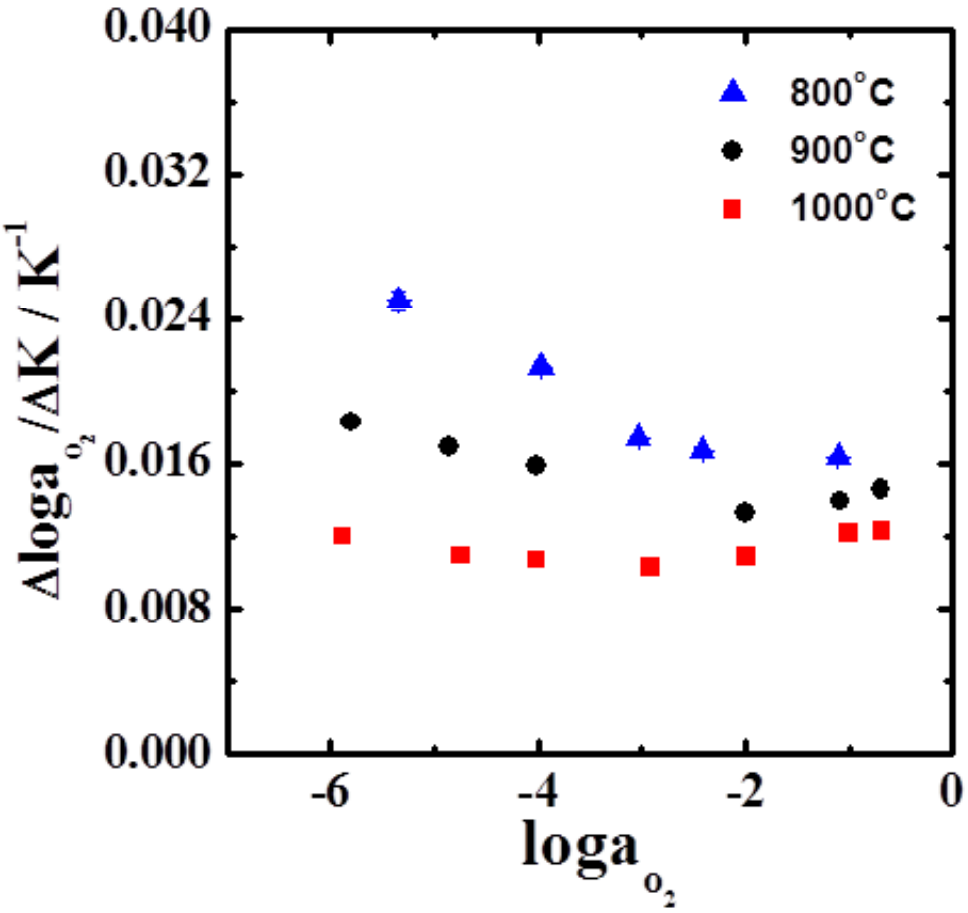

Fig.IV.9. $\Delta \log a_{o_2} / \Delta T$ vs. $\log a_{o_2}$ for temperature 800ºC, 900ºC, and 1000ºC

IV.2. Reduced Heat of Transport of Oxygen

Method of obtaining reduced heat of transport is based on former studies

Janek, Korte, and T. W. Lee [35-38]. As shown in Fig.IV.10, $-\Delta(\eta_i - \mu_o^{ref})/F$ with respect to ΔT, two different thermopowers (initial transient thermopower, θ^o, and steady state thermopower, θ^{st},) were obtained. Basically, difference between initial and steady state thermopower is originated from change in oxygen nonstoichiometry. From that difference, value of reduced heat of transport is calculated with Eq. (II.63). Method of acquiring initial and steady state thermopower is shown in Fig.IV.11. Then θ^o and θ^{st} data are plotted in Fig.IV.11 for three individual temperatures: 800ºC, 900ºC, and 1000ºC. Then reduced heat of transport data is plotted in Fig.IV.12.

From results interesting fact could be perceived. Initial and steady state thermopower show that their values increase as temperature decreases. Also for reduced heat of transport, its value is positive for temperature condition of 1000ºC while change is sign occurred when condition became T < 900ºC and 6 < loga_{O_2} < 2. From previous studies, reduced heat of transport induced by mobile atom can be expressed as function of reduced heat of transport of ionic and electronic defect and electrical conductivity of those species [35-37, 43]. It is suggested that the major reason of change in value of reduced heat of transport is due to movement of species with largest reduced heat of transport value and high electrical conductivity. But so far this term has not been vividly and quantitatively analyzed.

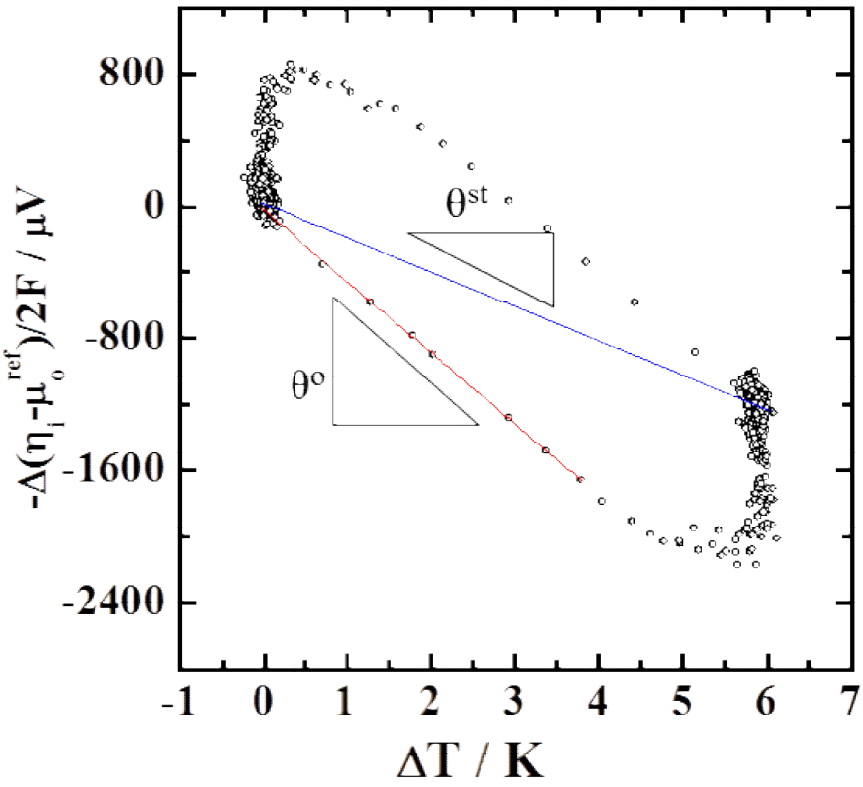

Fig.IV.10. $-\Delta(\eta_i - \mu_o^{ref})/F$ behavior with respect to ΔT along with calculation of initial, θ^o, and steady state, θ^{st}, ionic thermopower. Cell condition was at1000ºC in $\log a_{O_2} = \log a_{O_2}^{ref}$ = -1.985±0.001 where $\Delta T = T_2 - T_3$.

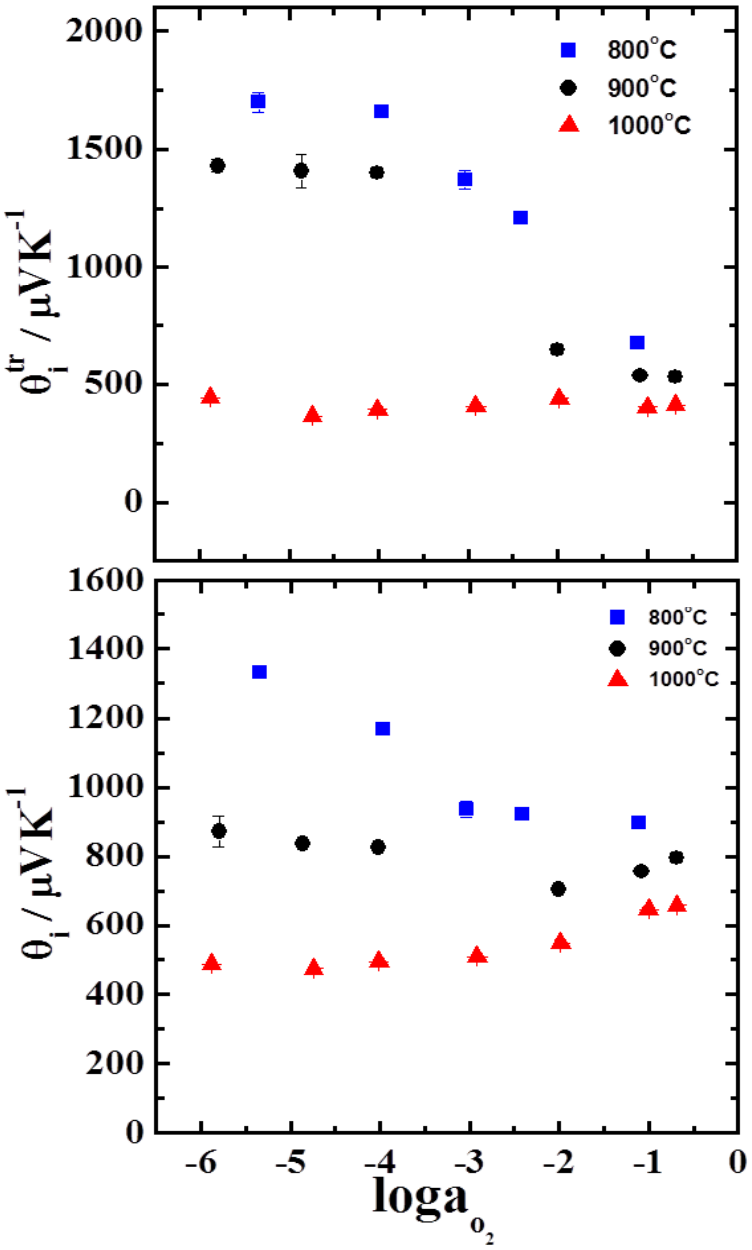

Fig.IV.11. Initial and steady state ionic thermopower vs. $\log a_{O_2}$ at 1000ºC, 900ºC, and 800ºC

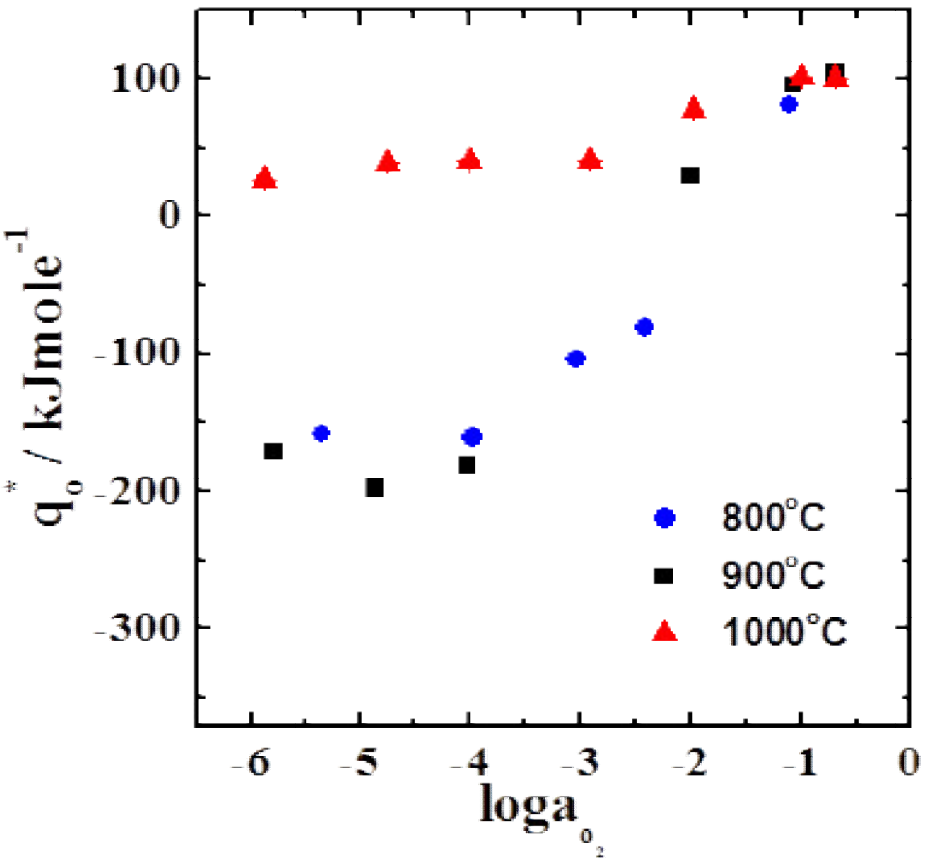

Fig.IV.12. reduced heat of transport vs. loga_{O_2} at 1000ºC, 900ºC, and 800ºC

IV.3 Analytic solution and its validity

When system placed under temperature gradient, movement of species does not solely depend on temperature but also on chemical diffusion. So for Soret experiment, dependence of chemical diffusion and temperature to time are studied to understand behavior of charged carriers inside the system. In section III.1.4, analytic solution has been stated. Compare to experiment performed by T.W. Lee [38], this experiment is different in fact that two-probe technique is used while 4-probe used technique is performed by T. W. Lee. So by modifying Eq. (II.66) and (II.67) into feasible form following equation is obtained.

$$-\frac{\Delta\eta_i(t,\Delta T)}{2F} = \frac{1}{2F}\left(\bar{S}_i + \frac{q_i^*}{T}\right)\Delta T - \frac{t_e}{2F}\frac{q_O^*}{T}\Delta T\left\langle \frac{8}{\pi^2}\sum_{n=1}^{\infty}(2n-1)^{-2}\exp\left[-\frac{(2n-1)^2\pi^2\tilde{D}(t-t_0)}{L^2}\right]\right\rangle \quad \text{(IV.5)}$$

With this simple solution, chemical diffusivity and reduced heat of transport values are obtained. Since behavior varies when $-6 < \log a_{O_2} < -2$ under temperature of 800ºC and 900ºC, for representative data, fitting results are plotted in Fig.IV.13 (1000ºC) and Fig.IV.14 (900ºC). These data are selected to show visual comparison of polarization direction which varies depend on thermodynamic conditions. As shown in Fig.IV.14, under $\log a_{O_2} = -4.018\pm0.001$ and $\log a_{O_2} = -5.799\pm0.001$ for temperature 900ºC, polarization direction changes that electrochemical potential decreases after thermal effect applied to the system. So in order to understand chemical polarization direction, $\Delta\mu_o$ is evaluated later.

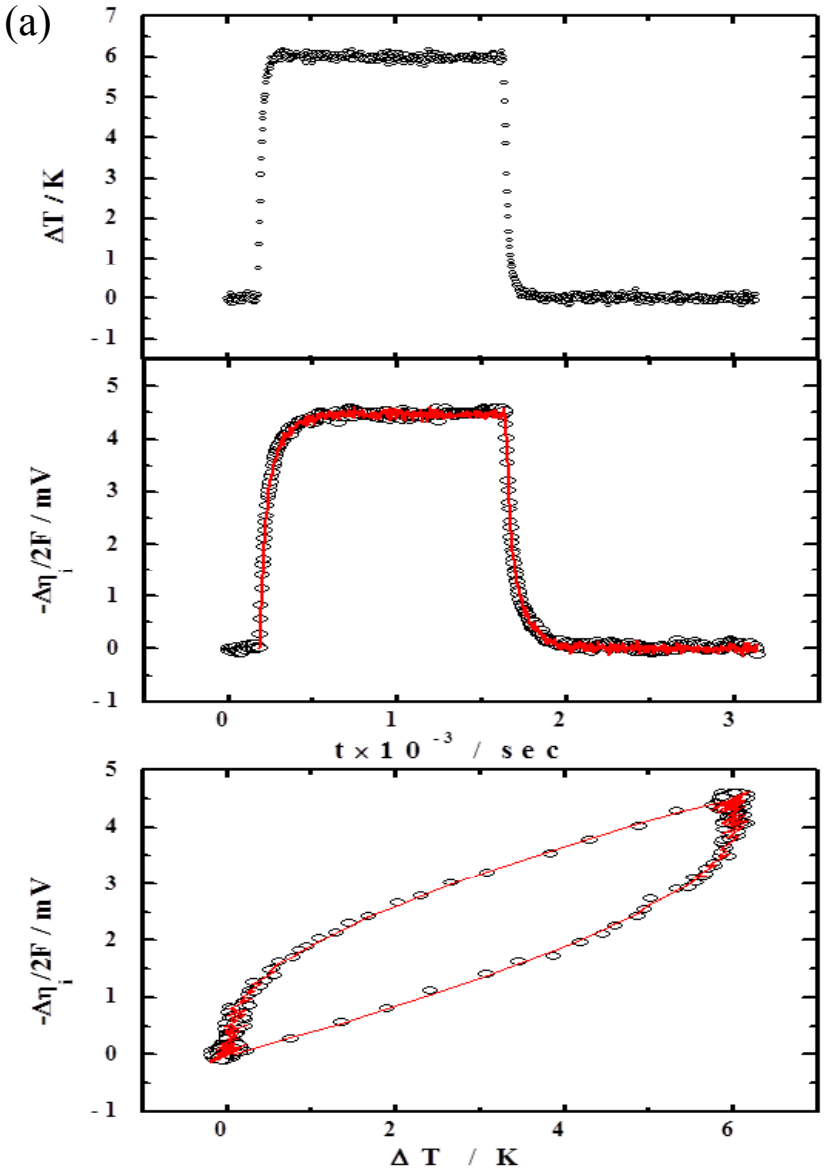

Fig.IV.13. Temporal behaviors of (top) $\Delta\eta_i/2F$ and (middle) ΔT against t with (bottom) $\Delta\eta_i/2F$ vs. ΔT for (a) $\log a_{O_2}$ = -1.003±0.001, (b) $\log a_{O_2}$ = -2.915±0.001 and (c) $\log a_{O_2}$ = -4.739±0.001 for temperature 1000ºC. Best-fitted curve with Eq. (IV.5) where L=0.529 cm.

(b)

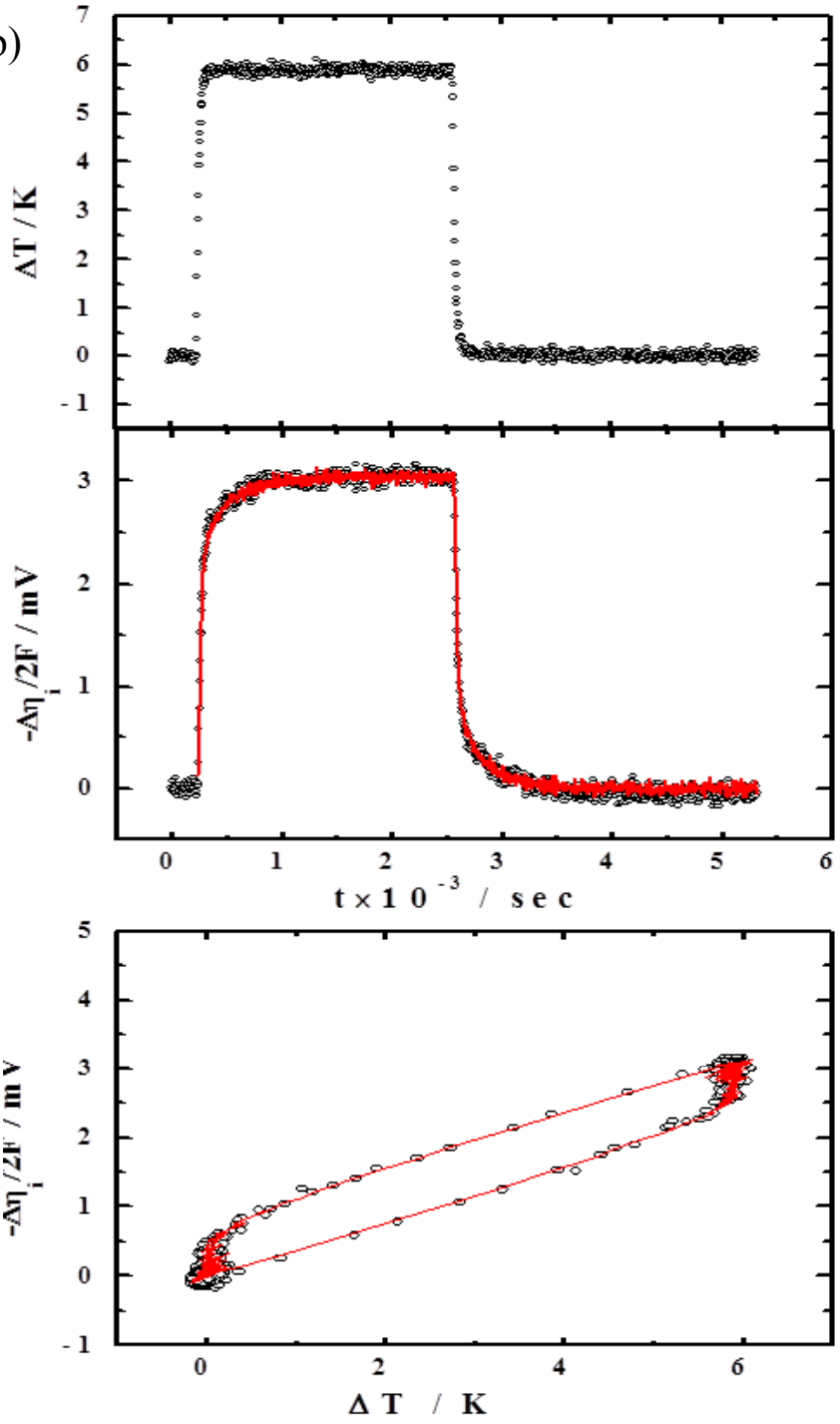

Fig.IV.13. (Continued)

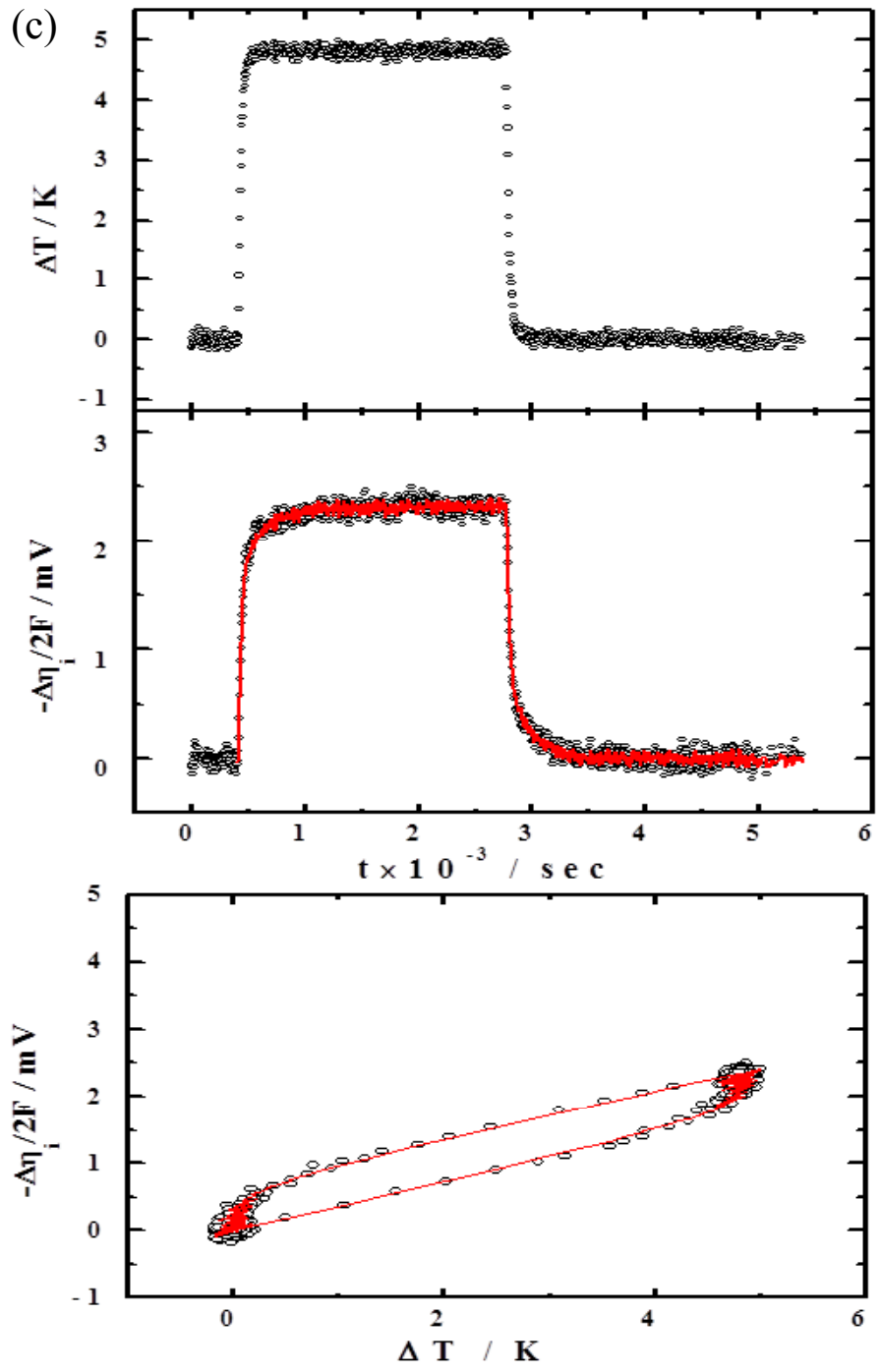

Fig.IV.13. (Continued)

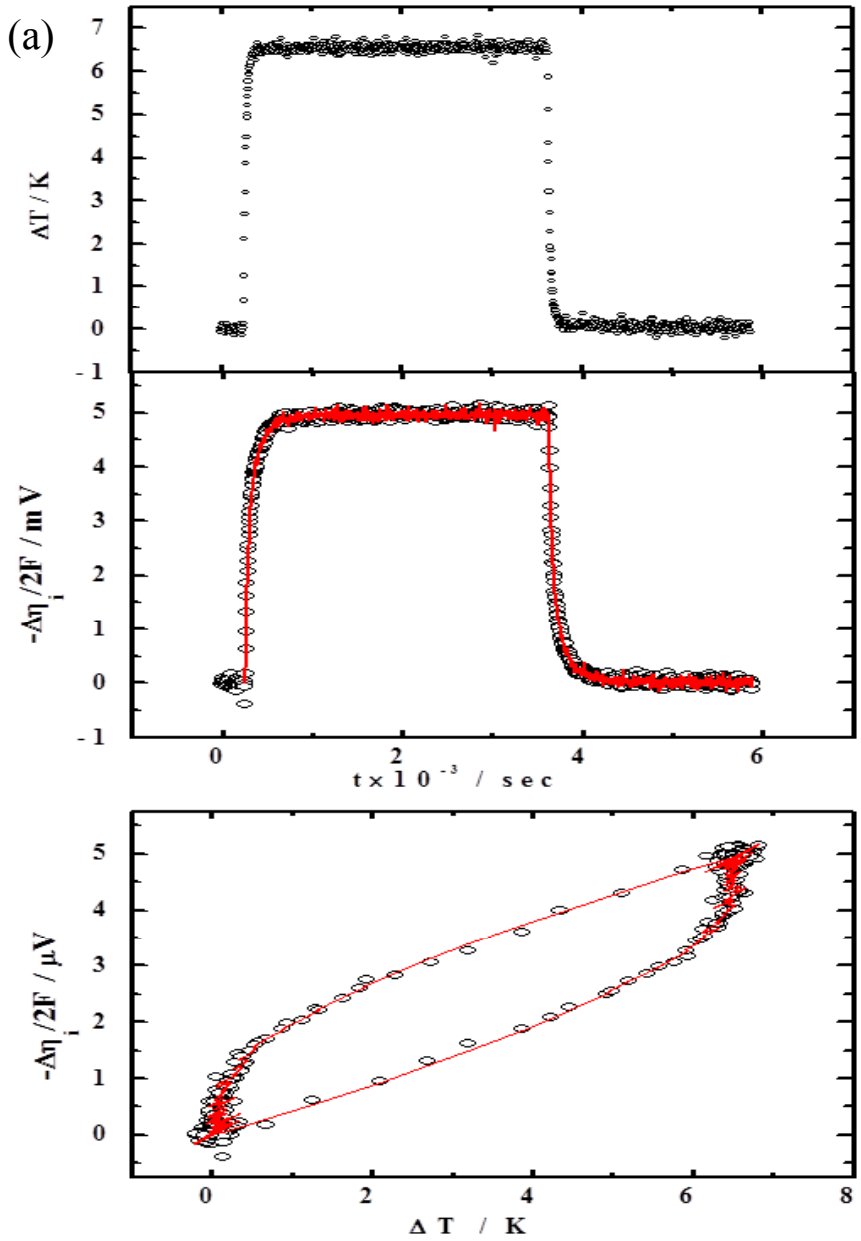

Fig.IV.14. Temporal behaviors of (top) $\Delta\eta_i/2F$ and (middle) ΔT against t with (bottom) $\Delta\eta_i/2F$ vs. ΔT for (a) $\log a_{O_2}$ = -1.079±0.001, (b) $\log a_{O_2}$ = -4.018±0.001 and (c) $\log a_{O_2}$ = -5.799±0.001 for temperature 900ºC. Best-fitted curve with Eq. (IV.5) where L=0.529 cm.

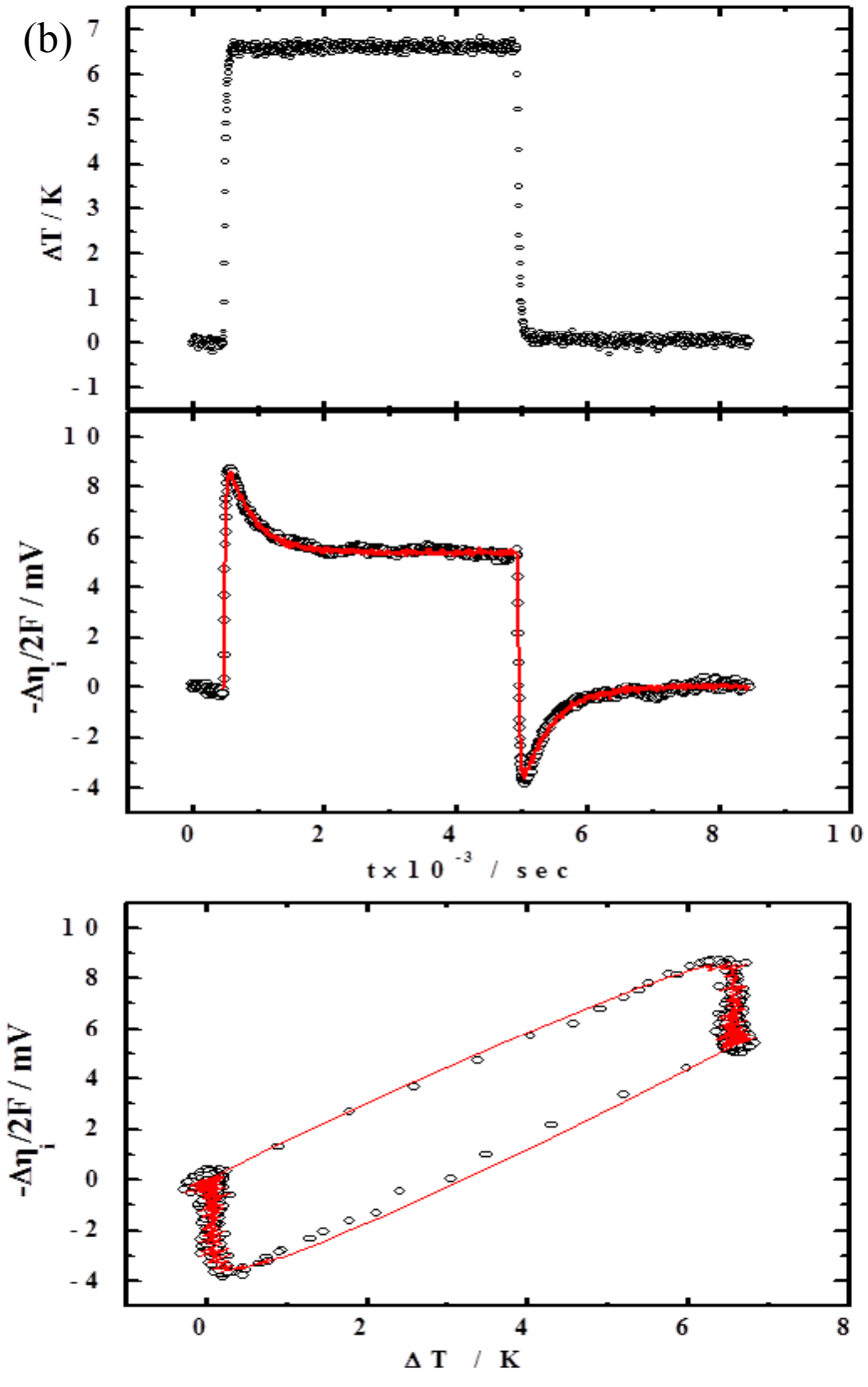

Fig.IV.14. (Continued)

(c)

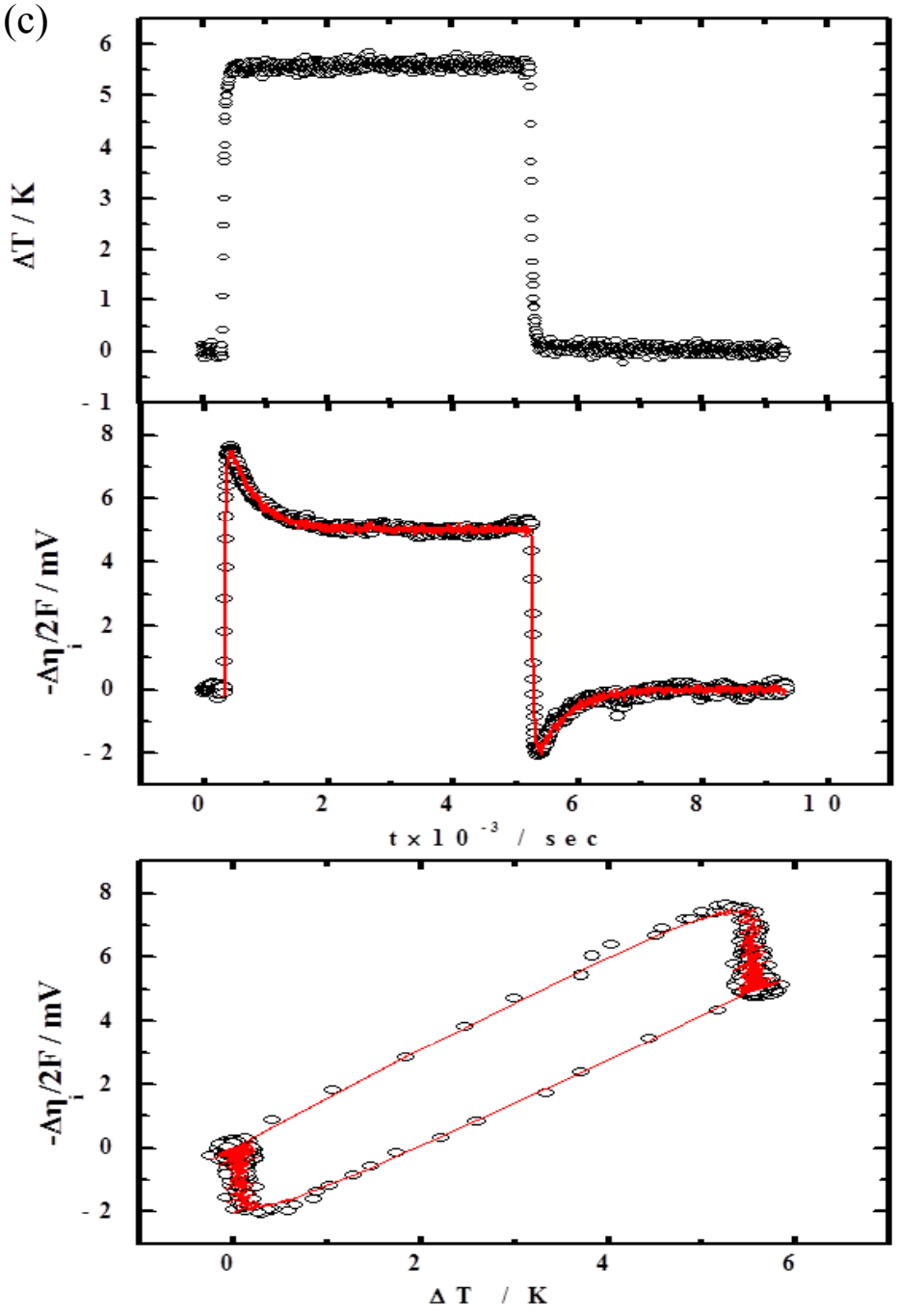

Fig.IV.14. (Continued)

From Eq. (IV.5), steady state thermopower, reduced heat of transport and chemical diffusivity data can be achieved. Analytic solution naturally contains lots of assumptions that can affect the obtained values deviated from true behavior of nature. So, by comparing obtained steady state thermopower from fitting and from linear regression, validity can be confirmed. Results are shown in Fig.IV.15 and the values obtained from linear regression and from analytic solution correspond to each other within error. Also, chemical diffusivity values are compared to that from previous work [16] to confirm the reliability of these data presented. Compared values of chemical diffusivity are presented in Fig.IV.16. Fig.IV.16 suggests that although chemical diffusivities were obtained from two individual cells, values correspond to each other within error. From this result, reliability of obtained data is confirmed. But for reduced heat of transport, values from linear regression and that from fitting seems to deviate as shown in Fig.IV.17. As mentioned earlier, reduced heat of transport can be calculated from initial and steady state thermopower as shown in Eq.(II.63). Since steady state thermopower values from linear regression and from analytic solution matches up with each other as shown in Fig.IV.15, reduced heat of transport value can give out different initial thermopower values obtained from linear regression process. So, there is problem in selecting which data is more reliable. But as mentioned earlier, analytic solution contains numerous assumptions that reduced heat of transport from linear regression can be more reliable. Further studies are required to understand this behavior.

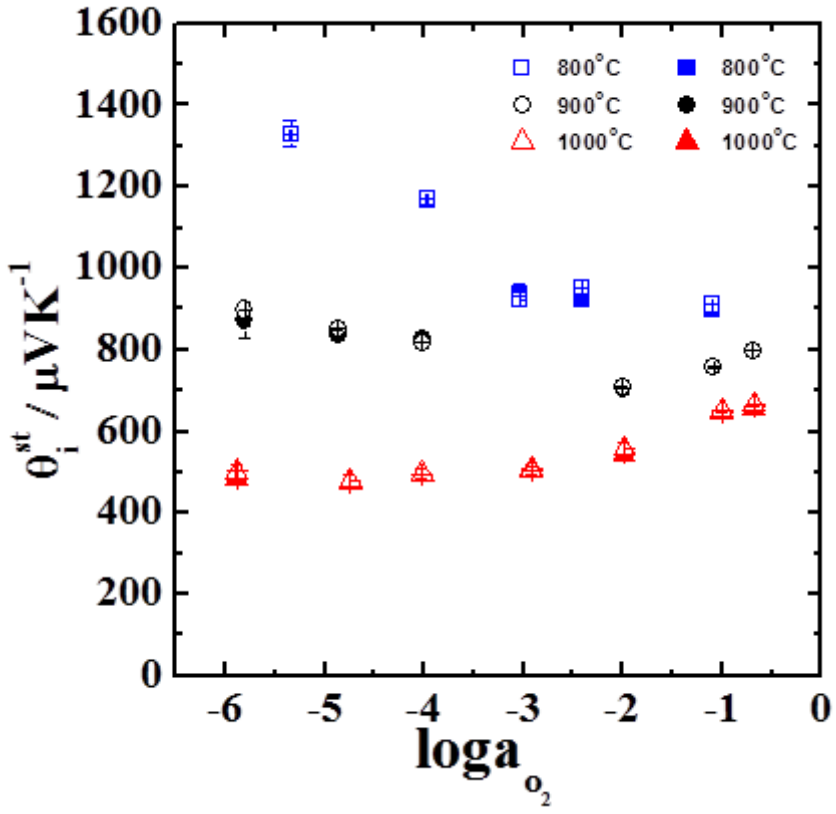

Fig.IV.15. Comparison of θ_i^{st} from fitting results off analytic solution (open symbol) and from linear regression (closed symbol).

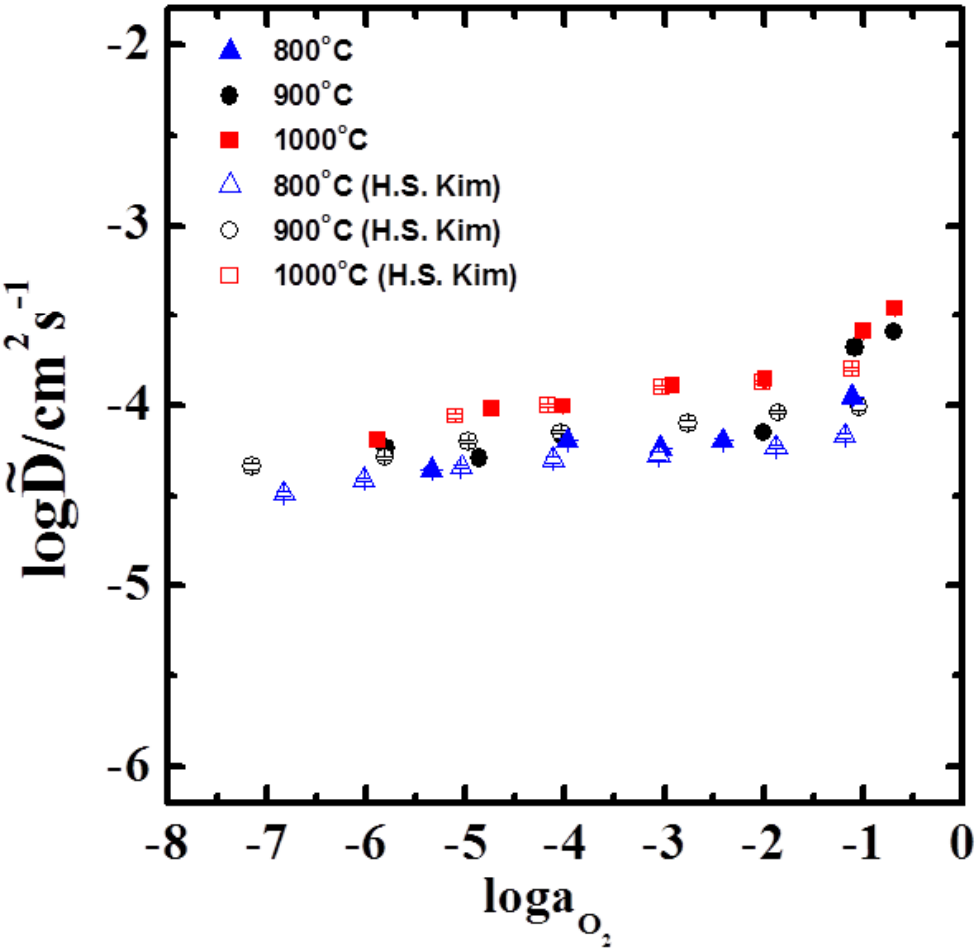

Fig.IV.16. Comparison of $\tilde{D}_o$ evaluated by simple solution compared to previous data from H.-S.Kim and H.-I. Yoo[16].

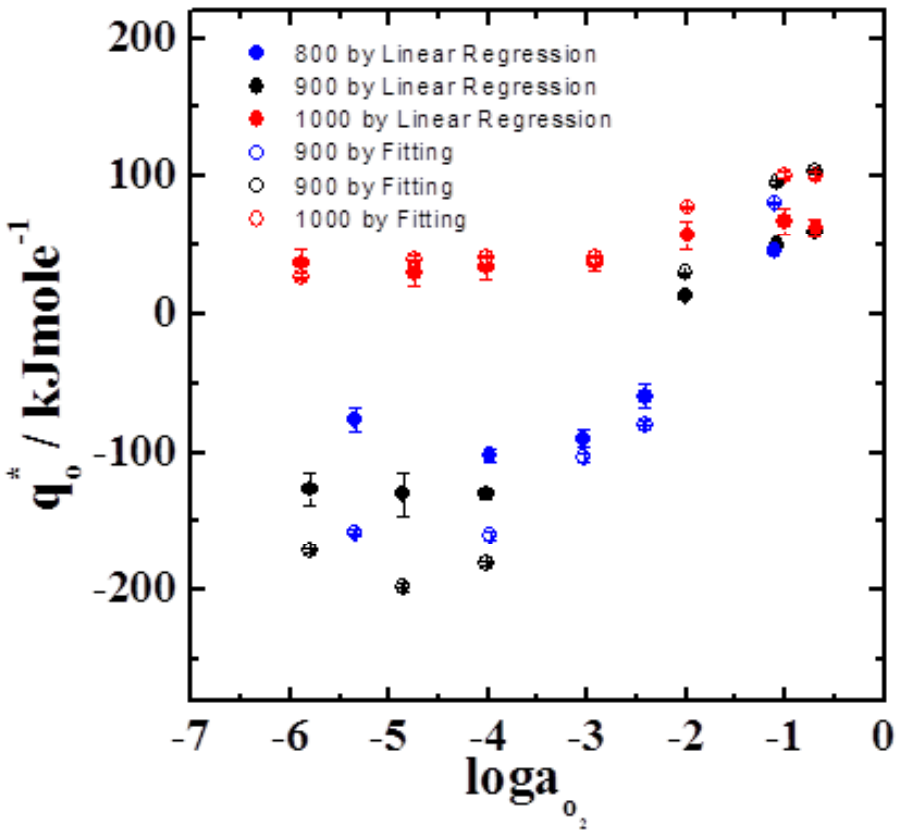

Fig.IV.17. Comparison of q_o^* evaluated from analytic solution (open symbol) and from linear regression (closed symbol).

IV.4 Thermomigrational Flux of O and Chemical Potential Equivalent to T Gradients

As previously mentioned, polarization of oxygen differs with respect to thermodynamic conditions. To understand true behavior of oxygen, chemical potential difference from top and bottom of the specimen is evaluated. Information on movement of oxygen ion is due to entropic effect and due to heat itself as shown in Eqs. (II.44), (II.61), and (II.62). From the analysis of non-isothermal transport coefficient, it is understood that oxygen ion moves from hot side to cold site when temperature gradient is applied to the system. Discard entropic effect, reduced heat of transport values suggested that oxygen ion movement based only on heat happens to be not always in the same direction which will be discussed later. So in order to navigate deeply into system, chemical potential from top and bottom of electrodes are explored. Similar to Eqs. (III.4-12), basic principle of experiment is as follows with symbols used are shown in Fig.IV.18. Starting with signals obtained from cell,

$$-\mathrm{F}U_{21} = \eta_{\mathrm{e,mu'}}(\mathrm{T_{ref}}) - \eta_{\mathrm{e,md'}}(\mathrm{T_{ref}}), \tag{IV.6}$$

, by transforming Eq. (IV.6) into Eq. (IV.7),

$$\begin{aligned} -\mathrm{F}U_{21} = \eta_{\mathrm{e,mu'}}(\mathrm{T_{ref}}) - \eta_{\mathrm{e,1}}(T_1) + \eta_{\mathrm{e,1}}(T_1) \\ -\eta_{\mathrm{e,2}}(T_2) + \eta_{\mathrm{e,2}}(T_2) - \eta_{\mathrm{e,md'}}(\mathrm{T_{ref}}) \end{aligned} \tag{IV.7}$$

, Eq. (IV.8) can be obtained with Eq. (III.6).

$$-\mathrm{F}U_{21} = \eta_{\mathrm{e},1}(T_1) - \eta_{\mathrm{e},2}(T_2) - \mathrm{F}\int_{T_2}^{T_1} \theta^{\mathrm{Pt}}\mathrm{d}T \tag{IV.8}$$

Similarly, Eq. (IV.8) can be written as Eq. (IV.9).

$$-\mathrm{F}U_{21} = \eta_{\mathrm{e},1}(T_1) - \eta_{\mathrm{e},1}(T_2) + \eta_{\mathrm{e},1}(T_2) - \eta_{\mathrm{e},2}(T_2) - \mathrm{F}\int_{T_2}^{T_1} \theta^{\mathrm{Pt}}\mathrm{d}T \tag{IV.9}$$

Substituting Eq. (III.7) into Eq. (IV.9), Eq. (IV.10) can be obtained.

$$-\mathrm{F}U_{21} = \mathrm{F}\int_{T_2}^{T_1} \theta^{\mathrm{YSZ}}\mathrm{d}T + \eta_{\mathrm{e},1}(T_2) - \eta_{\mathrm{e},2}(T_2) - \mathrm{F}\int_{T_2}^{T_1} \theta^{\mathrm{Pt}}\mathrm{d}T \tag{IV.10}$$

With Eq. (II.46) Eq. (IV.10) turns into Eq. (IV.11).

$$\begin{aligned} -\mathrm{F}U_{21} = \mathrm{F}\int_{T_2}^{T_1} \theta^{\mathrm{YSZ}}\mathrm{d}T &+ \frac{1}{2}\left[\mu_{\mathrm{o},1}(a_{\mathrm{o}_2}, T_2) - \eta_{\mathrm{i},1}(T_2)\right] \\ &- \frac{1}{2}\left[\mu_{\mathrm{o},2}(a_{\mathrm{o}_2}, T_2) - \eta_{\mathrm{i},2}(T_2)\right] - \mathrm{F}\int_{T_2}^{T_1} \theta^{\mathrm{Pt}}\mathrm{d}T \end{aligned} \tag{IV.11}$$

Since for pure ionic conductor, $\nabla\eta_{\mathrm{i}} \approx 0$, from Eq. (IV.11), chemical potential at position 2 can be written as Eq. (IV.12)

$$\mu_{o,3}(a_{o_2}, T_3) = 2FU_{34} + \mu_{o,4}(a_{o_2}, T_3) - 2F\theta^{YSZ}(T_3 - T_4) + 2F\int_{T_4}^{T_3} \theta^{Pt} dT \quad \text{(IV.12)}$$

Similarly, for U_{34}, starting with Eq. (IV.13),

$$FU_{34} = \eta_{e,mu'}(T_m) - \eta_{e,md'}(T_m) \quad \text{(IV.13)}$$

, chemical potential at position 3 can also be expressed as Eq. (IV.14).

$$\mu_{o,2}(a_{o_2}, T_2) = 2FU_{21} + \mu_{o,1}(a_{o_2}, T_2) + 2F\theta^{YSZ}(T_1 - T_2) - 2F\int_{T_2}^{T_1} \theta^{Pt} dT \quad \text{(IV.14)}$$

Then by subtracting (IV.12) from (IV.14), $\Delta\mu_o$ can be expressed as follows.

$$\mu_{o,2}(a_{o_2}, T_2) - \mu_{o,1}(a_{o_2}, T_2) = 2FU_{21} - 2FU_{34} + \mu_{o,1}(a_{o_2}, T_2) - \mu_{o,4}(a_{o_2}, T_2) + 2F\theta^{YSZ}(\Delta T' - \Delta T) - 2F\int_{T_2}^{T_1} \theta^{Pt} dT - 2F\int_{T_4}^{T_3} \theta^{Pt} dT \quad \text{(IV.15)}$$

The same as Section.III.5, all the other terms are corrected to left with $\mu_{o,2}(a_{o_2}, T_2) - \mu_{o,1}(a_{o_2}, T_2)$ [40-42].

This analysis is performed since interesting abnormal behavior of reduced heat of transport was show at 800ºC and 900ºC. Since sign of reduced heat of transport varies as in Fig.IV.12 and it can be visualized when plotting $\Delta\mu_o$ vs. ΔT. To visualize information contents for change in sing of heat of transport, schematic diagram is shown in Fig.IV.19. Initial transient state gives information of partial molar entropy of oxygen ($\bar{S}_o$) and steady state gives out information of transported entropy ($\bar{\bar{S}}_o$).

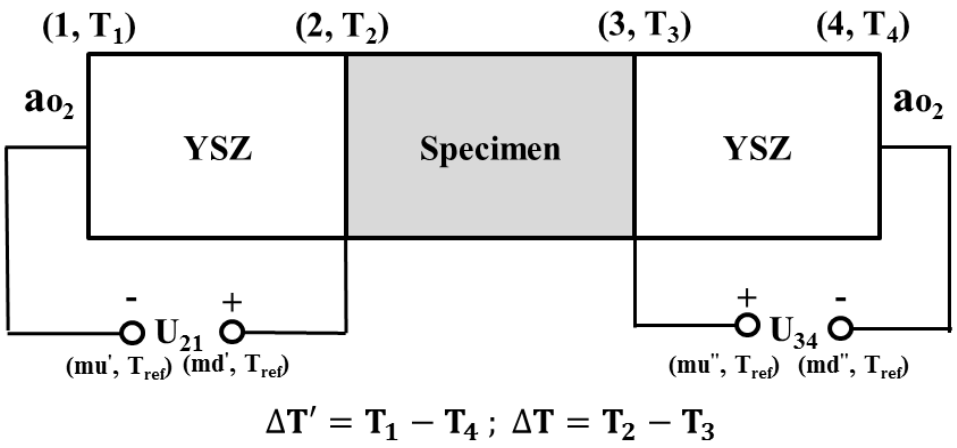

Fig.IV.18. Schematic of galvanic cell configuration for obtaining chemical potential from upper (position 2) and bottom (position 3) of specimen. Number and symbol in parenthesis each refers to position and temperature at that position. Temperature symbolism corresponds to that of Fig.III.7.

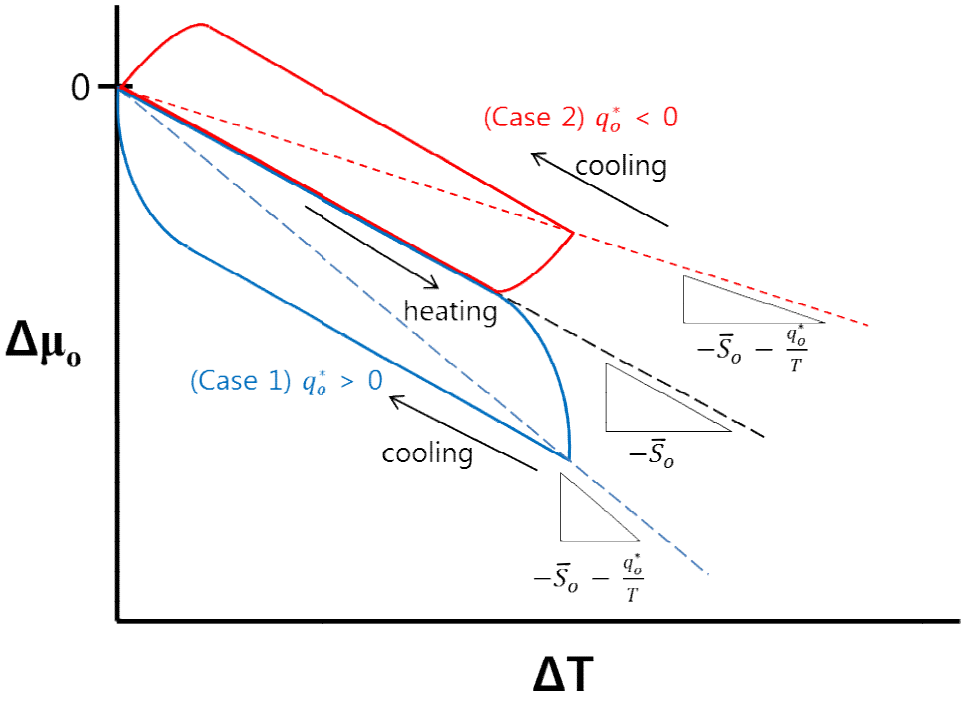

Fig.IV.19. Schematic diagram of $\Delta\mu_o$ vs. ΔT when sign of reduced heat of transport varies.

Similar to Fig.IV.19, actual experimental data showed equal trend in shape. Fig. IV.20 shows $\Delta\mu_o$ vs. ΔT data for both reduced heat of transport (q_o^*) value greater and less than zero. Two representative data were selected and presented in Fig.IV.20 with temperature condition of 800ºC where $\log a_{O_2}$ = -1.104 ± 0.001 (q_o^*>0) and $\log a_{O_2}$ = -3.031 ± 0.001 (q_o^*<0). Then as shown in Fig.IV.19, from slope of initial and steady state values, $-\bar{S}_o$ and $-\bar{S}_o - q_o^*/T$ were obtained. Then by subtracting $-\bar{S}_o$ from $-\bar{S}_o - q_o^*/T$, q_o^*/T value was retrieved and q_o^* finally was measured. For different oxygen activity condition, $-\bar{S}_o$, $-\bar{\bar{S}}_o$, and q_o^* are listed on Table.IV.1.

Table.IV.1. Measured $-\bar{S}_o$, $-\bar{\bar{S}}_o$, and q_o^* values under different oxygen activity at 800ºC.

$\log a_{O_2}$	$-\bar{S}_o$ (Jmol^{-1}K^{-1})	$-\bar{\bar{S}}_o$ (Jmol^{-1}K^{-1})	q_o^* (kJmol^{-1})
-1.104 ± 0.001	-197 ± 3	-257 ± 5	64 ± 6
-2.414 ± 0.001	-378 ± 18	-318 ± 16	-60 ± 30
-3.031 ± 0.001	-354 ± 18	274 ± 10	-90 ± 20
-3.970 ± 0.001	-436 ± 18	327 ± 13	-130 ± 20

Although this analysis shows large error, compare to value reduced heat of transport values obtained from initial and steady state partial thermopower, within error, values corresponds to each other. From this analysis, it can be visualized that discard oxygen ion movement derived by entropic effect, when it comes to pure temperature effect on oxygen ion, oxygen ion moves from cold side to hot side under condition $\log a_{O_2}$ < -2 when T $\leq$ 900ºC.

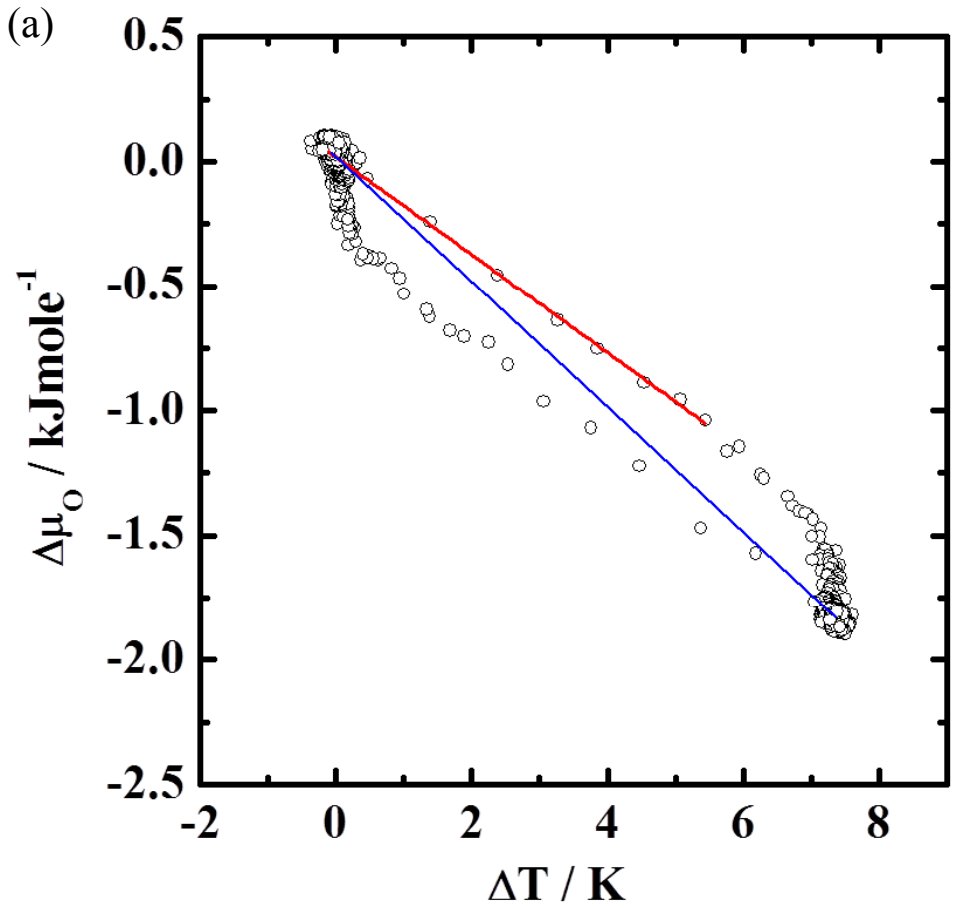

Fig.IV.20. $\Delta\mu_o$ calculated via Eq. (IV.15) from signals obtained from Fig.IV.16 vs. ΔT for (a) $\log a_{O_2}$ = -1.104 ± 0.001 ($q_o^* > 0$) and $\log a_{O_2}$ = -3.031 ± 0.001 ($q_o^* < 0$). Information retrieved from red line (initial transient state) refers to $-\bar{S}_o - q_o^*/T$ and information from blue line (steady state) refers to $-\bar{S}_o$, respectively.

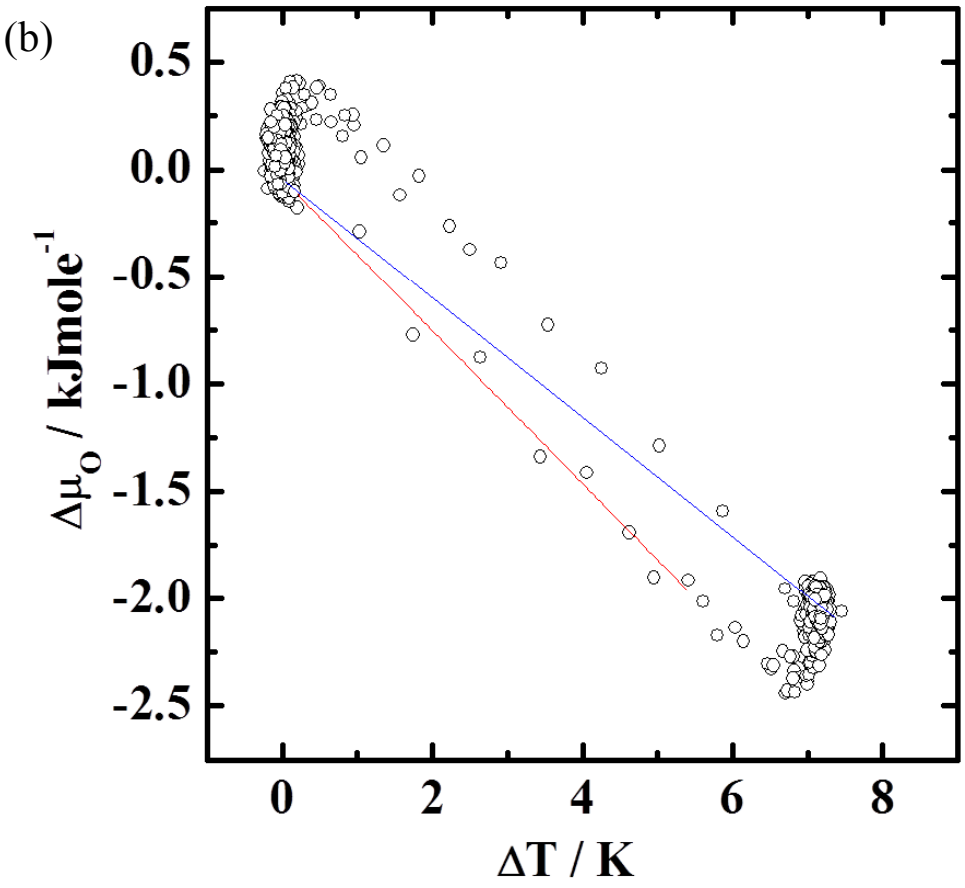

Fig.IV.20. (continued)

VI. Summary and Conclusion

From this work, mass and charge transport properties of $La_2NiO_{4+\delta}$ under temperature gradient is studied. Measurements are performed under temperature range of 800 ~ 1000ºC, as a function of $-6 < \log a_{O_2} < 0$.

Under these measurement conditions, initial transient partial ionic thermopwer and partial ionic/electronic thermpowers under Soret condition are measured. Also, non-isothermal transport coefficients are calculated based on 2x3 Onsager transport matrix [23]. Then chemical diffusivity and reduced heat of transport values are obtained via analytic solution [23]. Especially for chemical diffusivities, values obtained from this work are compared to that of previous study [16]. Initial transient and steady state ionic thermopowers are measured for the first time in this system.

Non-isothermal transport coefficients show positive values. From the result, it is suggested that oxygen ion moves from the relatively hotter side to colder side when there is no chemical potential gradient. Also, reduced heat of transport values showed its variance in sign under different thermodynamic conditions. This fact implies that discard oxygen ion movement derived by entropic effect, oxygen ion moves from the colder side to hotter side under condition $\log a_{O_2} < -2$ when $T \leq 900$ºC under measured condition.

Due to lack of study on heat of transport, plausible meaning has not been clarified. So understanding meaning of reduced heat of transport and effect of temperature on oxygen ion thermotransport is yet remained to be unsolved problems.

References

[1] V. V. Kharton and F. M. B. Marques, "Mixed Ionic-Electronic Conductors: Effects of Ceramic Microstructure on Transport Properties," *curr. Opin. Solid St. M.*, **6**, 261-269 (2002).

[2] K. Terabe, T. Hasegawa, T. Nakayama, and M.Aono, "Quantized Conductance Atomic Switch," *Nature*, **433**, 47-50 (2005).

[3] D. B. Strukov, G. S. Snider, D. R. Steward, and R. S. Williams, "The Missing Memristor found," *Nautre,* **453**, 80-83 (2008).

[4] R. Waser, R. Dittmann, G. Staikov, and K. Szot, "Redox-Based Resistive Switching Memories-Nanoionic Mechanisms, Prospects, and Challenges,´ *Adv. Mater.*, **21**, 2632-2663 (2009).

[5] S. J. Skinner, "Characterization of $La_2NiO_{4+\delta}$ using In-Situ High Temperature Neutron Powder Diffraction," *Solid State Sci.*, **5**, 419-426 (2003).

[6] L. Minervini, R. W. Grimes, J. A. Kilner, and K. E. Sickafus, "Oxygen Migration in $La_2NiO_{4+\delta}$," *J. Mater. Chem.*, **10**, 2349-2354 (2000).

[7] A. Chroneos, D. Parfitt, J. A. Kilner, and R. W. Grimes, "Anisotropic Oxygen Diffusion in Tetragonal $La_2NiO_{4+\delta}$: Molecular Dynamics Calculation," *J. Mater. Chem.*, **20**, 266-270 (2010).

[8] M. Jost, in "Diffusion in Solids, Liquids, Gases," Ch.12, Academic Press Inc. New York, (1960).

[9] M. A. Dragan, "Defect Chemistry, Transport Properties and Thermodynamic Stability of Acceptor Doped and Undoped Layerd La_2NiO_4," Ph.D thesis, University of Aachen (2006)

[10] A. Rabenan and P. Eckerlin, "The K_2NiF_4 structure in La_2NiO_4," *Acta, Cryst.*, **11**, 304-305 (1958).

[11] J. D. Jorgensen et al., "Structure of the interstitial oxygen defect in La_2NiO_4," *Physical Review B*, **40[1]**, 2186-2199 (1989).

[12] Hiroyasu Tamura, Akihiko Hayashi and Yutaka Ueda, “Phase Diagram of $La_2NiO_{4+\delta}(0 \leq \delta \leq 0.18)$ II. Thermodynamics of excess oxygen, phase transitions ($0.06 \leq \delta < 0.11$) and phase segregation ($0.03 \leq \delta < 0.06$),” *Physica C*, **258**, 61-71 (1996).

[13] V. V. Kharton et. Al., “Surface-limited Oxygen Transport and Electrode Properties of $La_2Ni_{0.8}Cu_{0.2}O_4$,” *Solid State Ionics*, **131**, 329-336 (2000).

[14] H.-S. Kim, “Defect Structure and Mass and Charge Transport Properties of $La_2NiO_{4+\delta}$,” Ph.D thesis, Seoul National University (2011)

[15] H.-S. Kim and H.-I. Yoo, “Complete Representation of Isothermal Mass and Charge Transport Properties of Mixed Ionic-Electronic Conductor $La_2NiO_{4+\delta}$,”*Phys. Chem. Chem. Phys.,* **12**, 12951-12955 (2010)

[16] H.-S. Kim and H-IYoo, “Defect-chemical analysis of nonstoichiometry, conductivity and thermopower of $La_2NiO_{4+\delta}$,” *Phys. Chem. Chem. Phys.*, **12**, 4074-4713 (2010)

[17] S.R. de Groot, *Thermodynamics of Irreversible Processes,* North-Holad Publishing Co., Amsterdam, 1951.

[18] C. Wagner, “Equations for Transport in Solid Oxides and Sulfides of Transition Metals,” *Prog. Solid State. Chem.,* **10**, 3-16 (1975).

[19] R.E. Howard and A.B. Lidiard, “Matter Transport in Solid,” *Rep.Proc.Phys.,* **27**, 161-240(1964)

[20] H.-S. Kim and H.-I. Yoo, “Compilation of All the Isothermal Mass/Charge Trnasport Properties of the Mixed Conduction $La_2NiO_{4+\delta}$ at Elevated Temperatures,” *Phys. Chem. Chem. Phys.,* **13**, 4651-4658 (2011)

[21] T. Lee, H. –S. Kim, and H.-I. Yoo, “From Onsager to Mixed Ionic Electronic Conductors,” *Solid State Ionics,* Submitted.

[22] E.D. Eastman, “Thermodynamics of Non-Isothermal Systems,” *J. Am. Chem. Soc*., **48**, 1482-1493 (1926); “Theory of the Soret Effect,” *J. Am Chem. Soc.*, **50**, 283-291 (1928).

[23] T. W. Lee, “Mass/Charge Transport Properties under Iso/Non-

isothermal Conditions and Defect Structure of Mixed Conducting $BaCo_{0.7}Fe_{0.22}Nb_{0.08}O_{3-\delta}$," Ph.D thesis, Seoul National University (2013)

[24] K. G. Denbigh, *The thermodynamics of the steady state,* Methuen, London, 1951, Chap.2, pp. 11-24.

[25] H. Rickert, *Electrochemistry of Solids: An Introduction,* Springer-Verlag, Berlin Heidelberg New York, 1982, Chap. 12, pp.216-234

[26] H.-I. Yoo and H.-S. Kim, "Complete representation of isothermal mass and charge transport properties of mixed ionic electronic conductors," *Solid State Ionics*, **225**, 166-171 (2011).

[27] C. Wagner, "The Thermoelectric Power of Cells with Ionic Compounds Involving Ionic and Electronic Conduction," *Prog. Solid State Chem.*, **7**, 1-37 (1972).

[28] J. Chipman, "The Soret Effects," *J. Am. Chem. Soc.*, **48(10)**, 2577-2589 (1926)

[29] W. Shockley, "Some Predicted Effects of Temperature Gradients on Diffusion in Crystals," *Phys Rev.*, **91**, 1563-1564 (1953).

[30] A. D. LeClaire, "Some Predicted Effects of Temperature Gradients on Diffusion in Crystals," *Phys Rev.*, **93(2)**, 344 (1954).

[31] H.-I. Yoo, H. Schmalzried, M. Martin, and J.Janet, "Cross Effect between Electronic and Ionic Flows in Semiconducting Transition Metal Oxides," *Z. Phys. Chem. N. F.*, **168**, 129-142 (1990).

[32] K.-C. Lee and H.-I. Yoo, "Hebb-Wagner-type Polarization/Relaxation in the Presence of Cross Effect between Electronic and Ionic Flows in a Mixed Conductor," *J. Phys. Chem. Solids.*, **60**, 911-927 (1999).

[33] J. N. Agar, "The Rate of Attainment of Soret Equilibrium," *Trans, Faraday Soc.*, **53**, 167-178 (1957).

[34] J. N. Agar and W. G. Breck, "Thermal Diffusion Potentials and the Soret Effect," *Nature*, **175(4450)**, 298-299 (1995).

[35] J. Janek and C. Korte, “Study of the Soret Effect in Mixed Conductors by the Measurement of Ionic and Electronic Thermopower,” *Solid State Ionics.*, **92**, 193-204 (1996).

[36] C. Korte and J. Janek, “Nonisothermal Transport properties of α-Ag_2S; Partial Thermopower of Electrons and Ions, the Soret Effect and Heats of Transport,” *J. Phys, Chem. Solids.*, **58(4)**, 623-637 (1997).

[37]C. Korte and J.Janek, “Ionic Conductivity, Partial Thermopowers. Heats of Transport and the Soret Effect of α-$Ag_{2+\delta}Se$ – an Experimental Study,” *Z. Phys. Chem.*, **206**, 129-163 (1998).

[38] M. Katama and T. Esaka, “Thermodynamic descriptions of oxygen redistribution in a nuclear fuel pellet: Heat of transport of oxygen in mixed conductors,” *J. Appl. Electrochem.*, **24**, 390-395 (1994).

[39] R. A. Oriani, “Thermomigration in Solid Metals,” *J.Phys. Chem. Solids.*, **30**, 339-351 (1969).

[40] H.-I. Yoo and J.-H. Hwang, “Thermoelectric Behavior of Single Crystalline ZrO_2 (+8m/o Y_2O_3),” *J. Phys. Chem. Solids*, **53[7]**, 973-981 (1991)

[41] N. Cusack and P. Kendall, “The Absolute Scale of Thermoelectric power at High Temperature,” *Proc. Phys. Soc.* (London), **72[6]**, 898-910 (1958).

[42] IUPAC, Oxygen, *International Thermodynamic Table of the Fluid State-9*, Blackwell, Oxfkrd, 1987, pp.30-35.

[43] J. Janek and H. Timm, “Thermal Diffusion and Soret Effect in (U, Me)$O_{2+\delta}$: the Heat of Transport of Oxygen,” *J. Nucl. Mater.*, **255**, 116-127 (1998).

Appendix-Numerical Data

A.1. Partial electronic thermopower under Soret condition

A.1.1 1000ºC

$\log a_{O_2}$	STD	θ_e^{st} / μVK^{-1}	STD
-0.683	0.001	-53.1	0.5
-1.002	0.002	-59.4	0.3
-1.985	0.002	-75.7	0.5
-2.916	0.002	-98.0	0.5
-4.014	0.001	-127.9	0.6
-4.739	0.001	-158.2	0.4
-5.883	0.001	-198.7	0.7

A.1.2 900ºC

$\log a_{O_2}$	STD	θ_e^{st} / μVK^{-1}	STD
-0.690	0.001	-51.9	0.3
-1.079	0.001	-55.0	0.4
-2.002	0.001	-68.5	0.2
-4.078	0.001	-107.8	0.8
-4.860	0.001	-137.0	0.2
-5.800	0.001	-169.2	0.5

A.1.3 800ºC

$\log a_{O_2}$	STD	θ_e^{st} / μVK^{-1}	STD
-1.104	0.001	-42.9	0.1
-2.414	0.001	-54.8	0.2
-3.033	0.001	-65.4	0.3
-3.970	0.001	-71.8	0.2
-5.343	0.001	-126.5	0.4

A.2. Partial ionic thermopower

A.2.1 1000ºC

$\log a_{O_2}$	STD	θ_i^{st} / μVK^{-1}	STD	θ_i^{o} / μVK^{-1}	STD
-0.683	0.001	659	4	410	20
-1.002	0.002	647	8	400	40
-1.985	0.002	547	10	440	40
-2.916	0.002	508	4	410	20
-4.014	0.001	494	5	390	30
-4.739	0.001	474	6	370	40
-5.883	0.001	487	7	450	30

A.2.2 900ºC

$\log a_{O_2}$	STD	θ_i^{st} / μVK^{-1}	STD	θ_i^{o} / μVK^{-1}	STD
-0.690	0.001	796	3	531	7
-1.079	0.001	756	5	536	5
-2.002	0.001	706	5	648	9
-4.078	0.001	827	6	1400	20
-4.860	0.001	836	8	1410	70
-5.800	0.001	870	40	1430	30

A.2.3 800ºC

$\log a_{O_2}$	STD	θ_i^{st} / μVK^{-1}	STD	θ_i^{o} / μVK^{-1}	STD
-1.104	0.001	897	7	675	7
-2.414	0.001	923	6	1210	20
-3.033	0.001	940	20	1370	40
-3.970	0.001	1170	10	1660	20
-5.343	0.001	1330	10	1700	40

A.3. Reduced heat of Transport

A.3.1 1000ºC

$\log a_{O_2}$	STD	q_o^* / kJmole^{-1}	STD
-0.683	0.001	60	6
-1.002	0.002	60	9
-1.985	0.002	26	9
-2.916	0.002	25	6
-4.014	0.001	25	8
-4.739	0.001	26	9
-5.883	0.001	10	10

A.1.2 900ºC

$\log a_{O_2}$	STD	q_o^* / kJmole^{-1}	STD
-0.690	0.001	60	2
-1.079	0.001	50	2
-2.002	0.001	13	2
-4.078	0.001	-129	4
-4.860	0.001	-130	15
-5.800	0.001	-126	11

A.1.3 800ºC

$\log a_{O_2}$	STD	θ_e^{st} / μVK^{-1}	STD
-1.104	0.001	46	2
-2.414	0.001	-59	8
-3.033	0.001	-90	6
-3.970	0.001	-102	5
-5.343	0.001	-76	9

A.4 Chemical Diffusivity

A.4.1 1000ºC

$\log a_{O_2}$	STD	$\log(\widetilde{D} / cm^2 s^{-1})$	STD
-0.683	0.001	-3.45	0.01
-1.002	0.002	-3.59	0.01
-1.985	0.002	-3.86	0.01
-2.916	0.002	-3.89	0.01
-4.014	0.001	-4.01	0.01
-4.739	0.001	-4.02	0.01
-5.883	0.001	-4.19	0.01

A.4.2 900ºC

$\log a_{O_2}$	STD	$\log(\widetilde{D} / cm^2 s^{-1})$	STD
-0.690	0.001	-3.59	0.01
-1.079	0.001	-3.68	0.01
-2.002	0.001	-4.15	0.01
-4.078	0.001	-4.16	0.01
-4.860	0.001	-4.29	0.01
-5.800	0.001	-4.24	0.01

A.4.3 800ºC

$\log a_{O_2}$	STD	$\theta_e^{st} / \mu V K^{-1}$	STD
-1.104	0.001	-3.96	0.01
-2.414	0.001	-4.20	0.01
-3.033	0.001	-4.24	0.01
-3.970	0.001	-4.20	0.01
-5.343	0.001	-4.35	0.01

A.5. Non-isothermal transport coefficients

A.5.1 1000ºC

$\log aO_2$	STD	$\log(L_{iT}$ / molcm^{-1}s^{-1}K^{-1})	STD	$\log(L_{hT}$ / molcm^{-1}s^{-1}K^{-1})	STD
-0.683	0.001	-9.3	0.2	-7.6	0.2
-1.002	0.002	-9.4	0.1	-7.6	0.2
-1.985	0.002	-9.5	0.1	-7.6	0.1
-2.916	0.002	-9.7	0.1	-7.6	0.2
-4.014	0.001	-9.8	0.1	-7.5	0.1
-4.739	0.001	-9.9	0.1	-7.5	0.2
-5.883	0.001	-10.0	0.1	-7.5	0.2

A.5.2 900ºC

$\log aO_2$	STD	$\log(L_{iT}$ / molcm^{-1}s^{-1}K^{-1})	STD	$\log(L_{hT}$ / molcm^{-1}s^{-1}K^{-1})	STD
-0.690	0.001	-9.4	0.1	-7.5	0.1
-1.079	0.001	-9.5	0.1	-7.6	0.1
-2.002	0.001	-9.6	0.2	-7.5	0.2
-4.078	0.001	-9.7	0.2	-7.6	0.2
-4.860	0.001	-9.8	0.2	-7.5	0.1
-5.800	0.001	-9.9	0.2	-7.5	0.2

A.5.3 800ºC

$\log aO_2$	STD	$\log(L_{iT}$ / molcm^{-1}s^{-1}K^{-1})	STD	$\log(L_{hT}$ / molcm^{-1}s^{-1}K^{-1})	STD
-1.104	0.001	-9.6	0.1	-7.8	0.1
-2.414	0.001	-9.6	0.3	-7.5	0.1
-3.033	0.001	-9.7	0.1	-7.6	0.1
-3.970	0.001	-9.7	0.2	-7.6	0.2
-5.343	0.001	-9.8	0.3	-7.4	0.3

요약(국문초록)

현대사회에 기술이 발전하면서 환경문제가 발생하면서, 연구자들 사이에서 “녹색 에너지” 라는 개념이 대두되고 있다. 세계적인 환경 문제를 해결하기 위해서, Solid Oxide Fuel Cell를 통한 재생 에너지 사용이 대안으로 제시되었다. 본문에서는 Solid Oxide Fuel Cell 에 사용되는 Mixed Ionic Electronic Conductor의 물질 전하 나름 이동특성을 분석하였다.

MIECs의 상업적인 활용을 최근에 연구자들의 관심을 끌었는데, 이는 pumping/separation membrane 등 다양한 곳에서 사용된다. 그 중에서도 La_2NiO_4 계가 이 연구에서 분석하고자 하는 물질로 선택되었는데, 그 이유는 높은 이온/전자 이동특성을 가지고 있어서이다. 이 물질계에 대해선 다양한 연구가 진행되었는데 등온 상태에서의 물질 전하 나름 이동특성이 그 중 하나이다. 상업적으로 물질에 온도차이가 인가될 수 밖에 없음에도 불구하고, 비 등온 상태에서의 물질 전하 나름 이동특성은 아직까지 분석된 예가 전무하다.

그래서 이 연구에서는, 비 등온 상태에서의 물질 전하 나름 이동특성을 two-probe 이온 차단 기술을 사용하여서 측정하였다. 이 기술을 통하여서 이온/전자의 열기전력이 측정되었고 undoped La_2NiO_4내의 산소 이동특성 또한 분석하였다. 선행된 등온 상태에서의 물질 전하 나름 이동특성을 통하여서 2x3 Onsager 행렬의 나름 계수들 또한 계산되었고, 이를 통해 산소 이온과 정공이 뜨거운 부분에서 찬 부분으로 이동한다는 사실이 규명되었다. 또한, 온도 차이가 얼마만큼의 산소 포텐셜 차이로 나타내어 질 수 있는지 또한 계산되었다. 그 결과에 따르면, 100K 의 온도차이가 시편에 인가된다면, $\Delta \log a_{O_2}$ 가 로그 스케일로 1.5정도 차이가 난다는 사실을 확인하였다. 아울러서 실제로 산소 이온이 열에 의해 어떻게 움직이는지를 규명하는 reduced heat of transport 값이 계산되었고, 그 값은 열역학적 조건에 따라 −200 에서 100 kJ/mole 의 값을 가졌다. 마지막으로, 시편 양단의 화학 포텐셜 차이를 확인하여서 물질 내의 산소 이동 특성을 좀더 면밀히 분석하였다.

표재어: 혼합 전도체, Onsager 나름 계수 행렬, 비등온 물질/전하 나름특성, 부분 이온/전자 열기전력, 나름열, 산소 이동 특성

학 번: 2012-22543